

DISJOINT SPARSITY FOR SIGNAL SEPARATION AND APPLICATIONS TO HYBRID INVERSE PROBLEMS IN MEDICAL IMAGING

GIOVANNI S. ALBERTI AND HABIB AMMARI

ABSTRACT. The main focus of this work is the reconstruction of the signals f and g_i , $i = 1, \dots, N$, from the knowledge of their sums $h_i = f + g_i$, under the assumption that f and the g_i 's can be sparsely represented with respect to two different dictionaries A_f and A_g . This generalizes the well-known ‘‘morphological component analysis’’ to a multi-measurement setting. The main result of the paper states that f and the g_i 's can be uniquely and stably reconstructed by finding sparse representations of h_i for every i with respect to the concatenated dictionary $[A_f, A_g]$, provided that enough incoherent measurements g_i are available. The incoherence is measured in terms of their mutual disjoint sparsity.

This method finds applications in the reconstruction procedures of several hybrid imaging inverse problems, where internal data are measured. These measurements usually consist of the main unknown multiplied by other unknown quantities, and so the disjoint sparsity approach can be directly applied. As an example, we show how to apply the method to the reconstruction in quantitative photoacoustic tomography, also in the case when the Grüneisen parameter, the optical absorption and the diffusion coefficient are all unknown.

1. INTRODUCTION

Hybrid, or coupled-physics, inverse problems have been extensively studied over the last years, both from the mathematical and the experimental points of view. A hybrid imaging modality consists in the combination of two types of techniques, one exhibiting the high contrast of tissues and a second one providing high resolution. Thus, the main drawbacks of the standard imaging modalities can be overcome, at least theoretically. Many combinations have been considered, such as optical and acoustic waves (photoacoustic tomography [54]), electric currents and ultrasounds (ultrasound modulated EIT [8]) or microwaves and ultrasounds (thermoacoustic tomography [54]). The reader is referred to [7, 53, 16, 5, 6, 67] for a review on the mathematical aspects related to hybrid imaging problems.

In general, the inversion for such problems involves two steps. In the first step, an inverse problem related to the high resolution wave provides certain internal measurements. Such internal data are usually functionals of the unknown parameters and of certain solutions of partial differential equations (the unknowns are

Date: August 2, 2015.

2010 *Mathematics Subject Classification.* 35R30, 65N21, 65T60, 68U10.

Key words and phrases. Morphological component analysis, signal separation, sparse representations, disjoint sparsity, inverse problems, hybrid imaging, quantitative photoacoustic tomography.

This work was supported by the ERC Advanced Grant Project MULTIMOD-267184.

normally the coefficients of the PDE). In the second step, the unknown parameter has to be reconstructed from the knowledge of the internal measurements. This is sometimes referred to as the quantitative step, since the information on the tissue properties contained in the internal data is only qualitative. In this paper we suppose that the first inversion has been performed, and focus only on the second step.

The quantitative step is normally solved with PDE-based methods, by combining the internal data with the PDE modeling the problem. Such approach is sometimes very powerful in the reconstruction [21, 13, 16, 2, 3]. However, there may be difficulties in using these methods. First, the PDE model may be accurate only in some circumstances but not in others [16]. Second, even if the PDE model is accurate, there may be too many unknowns to have unique reconstruction [19]. Third, even in cases when the reconstruction is unique, this may require the differentiation of the data [13, 14, 1], which is known to be an unstable process, or may require additional assumptions to be satisfied [13, 1, 17, 14, 4].

The main focus of this paper is an alternative approach to such problem based on the use of sparse representations, as it was first done by Rosenthal et al. in quantitative photoacoustic tomography (QPAT) [64]. The internal data in a domain Ω can be often expressed as the product of the unknown(s) and an expression involving the solutions of the PDE. (For example, in QPAT the internal data have the form $H = \Gamma\mu u$, where Γ is the Grüneisen parameter, μ is the optical absorption and u is the light intensity.) Taking the logarithm, the inversion corresponds to recovering two functions f and g from the knowledge of their sum

$$h(x) = f(x) + g(x), \quad x \in \Omega.$$

This problem is, in general, clearly unsolvable. However, it is possible to exploit the different levels of smoothness of f and g . Indeed, since f represents a property of the medium, such as the log conductivity, it is typically highly discontinuous. On the other hand, g is an expression involving the solutions of a PDE, and as such enjoys higher regularity properties. As a consequence, f and g have different features, and this can be used to separate them by using a sparse representation approach.

Two signals $f, g \in \mathbb{R}^n$ can be reconstructed from the knowledge of their sum $h = f + g$ provided that they have different characteristics. More precisely, they need to be sparsely represented, i.e., with few atoms, with respect to two incoherent dictionaries A_f and A_g . This method is usually called “morphological component analysis” (MCA), and was introduced by Starck et al. in [69] (see [25, 45, 44, 50, 24, 23, 42, 56, 71, 60] for related works and [55] for a survey on the topic. In particular, Donoho and Kutyniok [42, 56] first provided a theoretical foundation of geometric image separation into point and curve singularities by using tools from sparsity methodologies. If compared to these works, the novelty of this paper lies in the particular structure of the measurements, as we now describe.

In this work, motivated by hybrid imaging techniques, where multiple measurements with the parameters fixed can be taken, we extend this method to a multi-measurement setting. In general terms, this corresponds to the reconstruction of f (and g_i) from the knowledge of their sums

$$h_i = f + g_i, \quad i = 1, \dots, N.$$

We prove that the MCA approach gives unique and stable reconstruction, provided that enough incoherent measurements g_i 's are available. The incoherence is measured in terms of their mutual disjoint sparsity. In vague terms, the atoms from A_g used to represent g_i should change for different measurements (see Definition 1 for the precise conditions). Numerical simulations show that taking several solutions to the relevant PDE yields the necessary incoherence.

As an example, we discuss the inversion for QPAT, both in the simpler case when $\Gamma = 1$ and in the case with non-constant Γ in the diffusive regime for light propagation. For the $\Gamma = 1$ case, this method has the advantages of being very robust to noise and of not requiring a particular model for light propagation, if compared to the PDE-based approaches [21, 18]. In the case when $\Gamma \neq 1$ there is no uniqueness in the reconstruction, even with multiple measurements [19]; if the parameters are piecewise constant, uniqueness can be guaranteed, but the inversion may be very sensible to noise [61]. We propose a combination of the disjoint sparsity signal separation method and of the PDE method, which provides a satisfactory reconstruction, without requiring piecewise constant parameters. Numerical simulations are provided.

This work is structured as follows. In Section 2 we recall the basic notions related to sparse representations and present the method of morphological component analysis. In Section 3, the signal separation method based on multiple measurements and disjoint sparsity is described in detail and the main reconstruction result is proved. The numerical implementation of the method, together with the possible choices for the dictionaries A_f and A_g in hybrid imaging, are discussed in Section 4. Next, this method is applied to hybrid imaging in Section 5, and several numerical simulations are provided. Some concluding remarks are contained in Section 6. The proofs of the uncertainty principles stated in Section 3 are given in Appendix A.

2. SPARSE REPRESENTATIONS AND MORPHOLOGICAL COMPONENT ANALYSIS

In this section, we introduce the basic notions related to sparse representations and morphological components analysis.

2.1. Introduction to sparse representations. This presentation follows [27]. Let n be the dimension of the signal space, namely we shall consider signals $f \in \mathbb{R}^n$. Since in this paper we shall consider only images, we should think of n as being the resolution of the image, namely $n = d \times d$, where d is the number of pixels in each row and column. However, in this section we shall use the more general notation $f \in \mathbb{R}^n$, and think of a signal as a column vector of length n . We now discuss how a signal can be represented as a superposition of given atoms in a fixed dictionary. More precisely, let $A \in \mathbb{R}^{n \times m}$ be a dictionary, namely a collection of m atoms, that are the column vectors of A . We assume $m \geq n$ and that A has full rank. Thus, it is always possible to express f as a linear combination of these atoms, i.e. to write

$$(1) \quad f = Ay$$

for some vector of coefficients $y \in \mathbb{R}^m$. The most common situation is when $m = n$ and A is an orthonormal basis: in this case the coefficient y is uniquely determined. However, the situation we are interested in is when $m > n$. In this case the dictionary A is redundant, since f can be represented in many different ways as a combination of the atoms in A . In other words, the system (1) is underdetermined and has many solutions $y \in \mathbb{R}^m$.

The key observation is that this non-uniqueness can be exploited by selecting the best representation y . One way to measure the quality of a representation y is given by its sparsity, which can be quantified by the number of non-zero coefficients of y

$$\|y\|_0 := \#\{\alpha \in \{1, \dots, m\} : y(\alpha) \neq 0\},$$

where the symbol $\#$ denotes the cardinality of a set. The representation (1) is called *sparse* if $\|y\|_0 \ll m$. From the theoretical point of view, the sparsest representation can be found by minimizing the following problem

$$(2) \quad \min_{y \in \mathbb{R}^m} \|y\|_0 \quad \text{subject to } Ay = f.$$

The practical search for the minimum poses highly non trivial difficulties, and the description of the main issues goes beyond the scope of this work. Algorithms such as Matching Pursuit [59] or Basis Pursuit [36] can often be successfully used to find the sparsest solution. More details will be given in Section 4.

The choice of the dictionary A clearly plays a fundamental role in this context. Indeed, a signal f admits a sparse representation with respect to a dictionary A if f can be written as combination of few atoms in A . Therefore, the dictionary A has to be chosen to capture the main features of the signals we consider. Many choices of dictionaries for images are available, and a detailed discussion is presented in Section 4.

In the presence of noise, it is helpful to consider a relaxation of (2) and to allow a small error between the signal f and its representation in terms of the atoms of A . Thus, the minimization problem becomes

$$\min_{y \in \mathbb{R}^m} \|y\|_0 \quad \text{subject to } \|Ay - f\|_2 \leq \varepsilon,$$

for some $\varepsilon > 0$, or equivalently

$$\min_{y \in \mathbb{R}^m} \|y\|_0 + \lambda \|Ay - f\|_2,$$

for a suitable Lagrange multiplier $\lambda > 0$.

2.2. Introduction to morphological component analysis (MCA). One of the relevant applications of sparse representations is related to the separation of a signal into its constitutive components, provided they have different features. We shall describe the method discussed in [69]. Suppose that a signal $h \in \mathbb{R}^n$ can be written as a sum

$$h = \tilde{f} + \tilde{g},$$

with $\tilde{f}, \tilde{g} \in \mathbb{R}^n$. The problem under consideration is the reconstruction of \tilde{f} and \tilde{g} from the knowledge of h , under the assumption that \tilde{f} and \tilde{g} have distinctive characteristics. This assumption can be expressed in terms of sparse representations. Namely, suppose that there exist two dictionaries $A_f \in \mathbb{R}^{n \times m_f}$ and $A_g \in \mathbb{R}^{n \times m_g}$ such that:

- (1) \tilde{f} can be sparsely represented with respect to A_f but not with respect to A_g ;
- (2) and \tilde{g} can be sparsely represented with respect to A_g but not with respect to A_f .

Under these heuristic conditions (which will be made precise below), a strategy to find \tilde{f} and \tilde{g} may be to find a sparse representation $y = \begin{bmatrix} y_f \\ y_g \end{bmatrix}$ of h with respect to the concatenated dictionary $A = [A_f, A_g]$ and then to write $f = A_f y_f$ and

$g = A_g y_g$. As we have seen before, the sparse representation y is the minimum of the minimization problem

$$\min_{y \in \mathbb{R}^{m_f + m_g}} \|y\|_0 \quad \text{subject to } [A_f, A_g] \begin{bmatrix} y_f \\ y_g \end{bmatrix} = h,$$

or, in the presence of noise, of

$$\min_{y \in \mathbb{R}^{m_f + m_g}} \|y\|_0 \quad \text{subject to } \|[A_f, A_g] \begin{bmatrix} y_f \\ y_g \end{bmatrix} - h\|_2 \leq \varepsilon.$$

Even though this procedure is successful in many practical cases [69, 48, 64], a proof of the correct reconstruction, i.e. $f = \tilde{f}$ and $g = \tilde{g}$, is only valid in an ideal situation, which we now describe. In the case when A_f and A_g are both orthonormal sets, the proof is based on the following uncertainty principle [47, Theorem 1].

Proposition 1. *Let $\{a_1, \dots, a_{m_A}\}$ and $\{b_1, \dots, b_{m_B}\}$ be two orthonormal sets of vectors in \mathbb{R}^n . Take a vector $h \in \mathbb{R}^n \setminus \{0\}$ and suppose it has the following representations*

$$h = A y_A = B y_B$$

with respect to $A = [a_1, \dots, a_{m_A}]$ and $B = [b_1, \dots, b_{m_B}]$. Then

$$\|y_A\|_0 + \|y_B\|_0 \geq 2/M,$$

where

$$(3) \quad M = \max_{i,j} |(a_i, b_j)_2|$$

is the mutual coherence.

We provide a proof for completeness.

Proof. Let S_A and S_B denote the supports of y_A and y_B , respectively. By assumption we have $y_B(j) = (h, b_j)_2 = \sum_{i \in S_A} y_A(i) (a_i, b_j)_2$, whence by Cauchy-Schwartz inequality we obtain $|y_B(j)| \leq \|y_A\|_2 \sqrt{\#S_A} M$. Thus, since $\|y_A\|_0 = \#S_A$ and $\|y_B\|_0 = \#S_B$, this implies

$$\|y_B\|_2 \leq \|y_A\|_2 \sqrt{(\#S_A)(\#S_B)} M \leq \|y_A\|_2 (\|y_A\|_0 + \|y_B\|_0) \frac{M}{2}.$$

This concludes the proof, since the orthonormality of A and B implies $\|y_A\|_2 = \|h\|_2 = \|y_B\|_2$ (Lemma 1 part 1). \square

In general, it is easy to see that if A and B are orthonormal bases then $1/\sqrt{n} \leq M \leq 1$ [45]. As a simple consequence of this result [47, Theorem 2], we have that if $y^1 \in \mathbb{R}^{2n}$ and $y^2 \in \mathbb{R}^{2n}$ are two representations of h with respect to the concatenated dictionary $A = [A_f, A_g]$, then

$$\|y^1\|_0 + \|y^2\|_0 \geq 2/M.$$

Therefore, if \tilde{f} and \tilde{g} have representations \tilde{y}_f and \tilde{y}_g satisfying $\|\tilde{y}_f\|_0 + \|\tilde{y}_g\|_0 < 1/M$, then the above method provides the correct reconstruction.

In practice, the assumption $\|\tilde{y}_f\|_0 + \|\tilde{y}_g\|_0 < 1/M$ is almost never satisfied, and so the above argument remains only a theoretical speculation. However, when the multi-measurement case is considered, correct and stable reconstruction can be rigorously proved. This theoretical result is also validated by several numerical simulations. These aspects are discussed in the following sections.

3. DISJOINT SPARSITY FOR MORPHOLOGICAL COMPONENT ANALYSIS

3.1. Introduction and main assumptions. Motivated by several hybrid imaging modalities (see Section 5), we generalize the MCA problem to a multi-measurement setting. The reader is referred to [25, 50, 24] for other similar variations.

Let $h_1, \dots, h_N \in \mathbb{R}^n$ be N signals that can be decomposed as

$$h_i = \tilde{f} + \tilde{g}_i, \quad i = 1, \dots, N,$$

with $\tilde{f}, \tilde{g}_i \in \mathbb{R}^n$. We want to study the problem of finding \tilde{f} and \tilde{g}_i from the knowledge of h_i for $i = 1, \dots, N$. The case $N = 1$ was discussed in the previous section. We shall show that as N becomes bigger, the above problem becomes much more treatable, and that the sparsity approach introduced before always provides the correct reconstruction, also in the presence of noise. As before, let A_f and A_g be the dictionaries with respect to which \tilde{f} and \tilde{g}_i have sparse representations, respectively. Note that all the \tilde{g}_i 's can be sparsely represented with the same dictionary A_g : this is a crucial assumption of this approach. Assume that the atoms of A_f are normalized to 1 and that

$$(4) \quad \text{the atoms of } A_g \text{ constitute an orthonormal set of } \mathbb{R}^n.$$

Thus, A_g can be completed to an orthonormal basis $[A_g, A_g^\perp]$ for some $A_g^\perp \in \mathbb{R}^{n \times (n-m_g)}$.

The reconstruction method applied to this case consists in the minimization of

$$(5) \quad \min_{y \in \mathbb{R}^{m_f + Nm_g}} \|y\|_0 \quad \text{subject to } \|A_f y_f + A_g y_g^i - h_i\|_2 \leq \varepsilon, \quad i = 1 \dots, N,$$

where we have used the notation $y = {}^t[y_f, {}^t y_g^1, \dots, {}^t y_g^N]$. Here, the superscript t denotes the transpose. To model the case with added noise, we write

$$(6) \quad h_i = \tilde{f} + \tilde{g}_i + n_i, \quad i = 1, \dots, N,$$

where \tilde{f} and the \tilde{g}_i 's represent the true signals, the h_i 's are the measured signals and n_i is such that

$$(7) \quad \|n_i\|_2 \leq \eta, \quad i = 1, \dots, N$$

for some small $\eta > 0$.

In the applications we have in mind (Section 5), the signal \tilde{f} represents (the logarithm of) a physical constitutive parameter, while the \tilde{g}_i 's usually quantify the injected fields, e.g., the electric field or the light intensity. As such, \tilde{f} is given and fixed, and we have no control on it. On the other hand, the \tilde{g}_i 's come from the measurements, and can be indirectly controlled. More precisely, the \tilde{g}_i 's depend on the solutions of a certain PDE, whose coefficients are unknown, but whose boundary values can be chosen: in this sense the \tilde{g}_i 's can be controlled. It is therefore natural to give some assumptions on the \tilde{g}_i 's.

The main requirements are that the \tilde{g}_i 's should be *sufficiently many and incoherent*¹. This will be mainly expressed by means of their disjoint sparsity with respect to A_g . (Disjoint sparsity was used in [24], while joint sparsity has been extensively used in compressive sensing [37, 35].) We shall therefore write

$$(8) \quad \|A_f \tilde{y}_f - \tilde{f}\|_2 \leq \rho_f, \quad \|A_g \tilde{y}_g^i - \tilde{g}_i\|_2 \leq \rho_g, \quad i = 1, \dots, N$$

¹Similar assumptions of enough independent measurements are required also when using PDE methods for hybrid inverse problems (see § 5.1).

for some $\rho_f, \rho_g > 0$. The approximation allows a small error between the true signals and their sparse representations. We shall prove that under suitable assumptions, a minimizer of (5) provides the correct reconstruction, up to a factor that is small in $\varepsilon := \rho_f + \rho_g + \eta$. In terms of the coefficient vectors $\{\tilde{y}_g^1, \dots, \tilde{y}_g^N\}$, the required assumptions can be written as follows.

Definition 1. Take $\beta, D > 0$, $N \in \mathbb{N}^*$, $\tilde{y}_f \in \mathbb{R}^{m_f}$ and $\tilde{y}_g^1, \dots, \tilde{y}_g^N \in \mathbb{R}^{m_g}$. We say that $\{\tilde{y}_g^1, \dots, \tilde{y}_g^N\}$ is a (β, D) -complete set of measurements if the following two conditions hold true:

CS1: if $|\tilde{y}_g^i(\alpha) - \tilde{y}_g^j(\alpha)| \leq \beta$ and $\tilde{y}_g^i(\alpha)\tilde{y}_g^j(\alpha) \neq 0$ for some $\alpha \in \{1, \dots, m_g\}$ then $i = j$;

CS2: for every $q \in \mathbb{R}^{m_f}$ such that $\|A_f q\|_2 > D$ and $\|{}^t A_g^\perp A_f q\|_2 \leq 2/3$ there holds

$$(9) \quad \#(\text{supp } q \setminus \text{supp } \tilde{y}_f) + \sum_{i=1}^N \#(S_q \setminus \text{supp } \tilde{y}_g^i) > \# \bigcup_{i=1}^N \text{supp } \tilde{y}_g^i + \|\tilde{y}_f\|_0,$$

where $S_q = \{\alpha : |({}^t A_g A_f q)(\alpha)| \geq 1\}$.

Let us comment on these two requirements. The first condition, CS1, is a constraint on the incoherence of the \tilde{g}_i 's in terms of the values of their coefficient vectors. More precisely, the coefficients relative to the same atom for two different \tilde{g}_i 's cannot be too close. This assumption could be relaxed by allowing a fixed number of \tilde{y}_g^i to have the same coefficients, but for simplicity of exposition we have decided to omit this generalization.

While CS1 is mainly a technical hypothesis, condition CS2 is the main assumption related to the disjoint sparsity of the \tilde{g}_i 's. Indeed, when the sets $\text{supp } \tilde{y}_g^i$ are small (the representation is sparse) and substantially change when i varies (disjoint), then it becomes possible to satisfy CS2 by taking N large enough, since the right-hand side is bounded by $\|\tilde{y}_f\|_0 + m_g$. Note that CS2 can always be satisfied by choosing the \tilde{y}_g^i so that $\#\{i : \tilde{y}_g^i(\alpha) = 0\} > \#\bigcup_i \text{supp } \tilde{y}_g^i + \|\tilde{y}_f\|_0$ for every α , but this represents only a worst case scenario. In general, the smaller $\text{supp } \tilde{y}_f$ and $\text{supp } \tilde{y}_g^i$ are, the easier it becomes to satisfy CS2.

Remark 1. It is expected that the number of measurements N should increase as the noise level η becomes bigger. Indeed, to have a good reconstruction, we need to keep $\varepsilon = \rho_f + \rho_g + \eta$ small. Thus, if the noise level η increases, the quantities ρ_f and ρ_g have to become smaller. In other words, the sparse approximations in (8) have to be more precise, which in turn requires the support of \tilde{y}_f and \tilde{y}_g^i to be bigger, and so a higher number of measurements is needed to satisfy CS2, as we heuristically observed above (see Example 1 below for a concrete example).

3.2. Uncertainty principles. As we have already pointed out, the smaller $\text{supp } \tilde{y}_f$ and $\text{supp } \tilde{y}_g^i$ are, the easier it becomes to satisfy CS2. Moreover, when A_f and A_g are two orthonormal bases, by Proposition 1 we have

$$\|q\|_0 + \|{}^t A_g A_f q\|_0 \geq 2/M,$$

where M is the mutual coherence of A_f and A_g defined in (3). However, this inequality is not directly applicable to our context, since $\|{}^t A_g A_f q\|_0$ does not appear explicitly in (9) and A_g will not be a basis in the applications. The following generalization of the uncertainty principle guarantees that the same bound holds, provided that D is big enough. The proof is given in Appendix A.1.

Proposition 2. *Assume that A_f is an orthonormal basis of \mathbb{R}^n and that A_g is an orthonormal set of \mathbb{R}^n and let M denote their mutual coherence. There exists $D > 0$ such that*

$$\|q\|_0 + \#\{\alpha : |({}^t A_g A_f q)(\alpha)| \geq 1\} \geq 2/M,$$

for every $q \in \mathbb{R}^n$ with $\|A_f q\|_2 > D$ and $\|{}^t A_g^\perp A_f q\|_2 \leq 2/3$.

Remark 2. In the single measurement case (if A_f is an orthonormal basis), CS1 and CS2 correspond to the condition $\|\tilde{y}_f\|_0 + \|\tilde{y}_g\|_0 < 1/M$, thereby reobtaining the hypothesis discussed in the previous section. Indeed, if $N = 1$ then CS1 is immediately satisfied. Moreover, CS2 becomes

$$\#\text{supp } q \setminus \text{supp } \tilde{y}_f + \#\{\alpha : |({}^t A_g A_f q)(\alpha)| \geq 1\} \setminus \text{supp } \tilde{y}_g > \|\tilde{y}_g\|_0 + \|\tilde{y}_f\|_0.$$

By Proposition 2, the left hand side is bounded by below by $2/M - (\|\tilde{y}_f\|_0 + \|\tilde{y}_g\|_0)$, and so the above inequality is satisfied provided that $\|\tilde{y}_f\|_0 + \|\tilde{y}_g\|_0 < 1/M$.

The more incoherent the two bases are, the bigger $2/M$ is, and therefore the bigger the left-hand side in (9) is. It is not a surprise that the incoherence of the bases makes these assumptions easier to be satisfied, since this was the starting point of the MCA discussed in the previous section.

Let us discuss a simple example to show the relation between the sparsity of the coefficients and the number of measurements N .

Example 1. Let us consider the simplest problem of the separation of spikes and sinusoids in 1D. Let $A_f = I_n \in \mathbb{R}^{n \times n}$ be the identity matrix and A_g be the Fourier basis. Their mutual coherence is $M = 1/\sqrt{n}$. Let $\tilde{y}_f \in \mathbb{R}^n$ be such that $\|\tilde{y}_f\|_0 = k$ and $\tilde{y}_g^i \in \mathbb{R}^n$ be such that $\|\tilde{y}_g^i\|_0 = l$ and with disjoint support, for $i = 1, \dots, N$. We would like to investigate the link between the number of measurements N and the sparsity of \tilde{y}_f and \tilde{y}_g^i , i.e. with the quantities k and l .

Thanks to the assumption on the supports of the \tilde{y}_g^i 's, condition CS1 is automatically satisfied for any $\beta > 0$. As far as CS2 is concerned, unfortunately we cannot check its validity for all possible choices of q . Thus, we make an heuristic choice with one of the worst possibilities, the Dirac comb, for which the inequality of the uncertainty principle becomes an equality. Set $q_\delta(\alpha) = 1$ when α is a multiple of \sqrt{n} and $q_\delta(\alpha) = 0$ otherwise. It turns out that $A_g q_\delta = q_\delta$, and so $\|q_\delta\|_0 = \#S_{q_\delta} = \sqrt{n}$. Provided that $l < \sqrt{n}$, it turns out that condition CS2 for y_δ is satisfied if

$$\frac{2k}{N+1} + l < \sqrt{n}.$$

Thus, the bigger the number of measurements is, the bigger k and l can be.

Assume now that A_g contains only a subset of the Fourier basis of cardinality m_g (as we shall do in the numerical simulations), and select a vector q_δ such that $\|q_\delta\|_0 = \#S_{q_\delta} = \sqrt{n}$ as before. Thus, CS2 is satisfied if

$$2k < N(\sqrt{n} - l) + \sqrt{n} - m_g,$$

independently of the supports of the \tilde{y}_g^i 's. For a fixed $l < \sqrt{n}$, the higher N is, the bigger k can be.

When considering wavelets and the Fourier basis, as in the numerical simulations of this paper, there is the added difficulty that the mutual coherence is not small, but in fact of order 1, which makes the uncertainty principle discussed above of no

practical use. However, if we consider Haar wavelets and low frequency trigonometric polynomials, as in Section 5, it is possible to improve this bound (a similar result for spikes and sinusoids is given in [46, Lemma 1]). We now discuss this result.

We consider two dimensional signals in \mathbb{R}^n , where $n = d \times d$ and $d = 2^J$ for some $J \in \mathbb{N}^*$. Let A_f be the associated orthonormal basis consisting of 2D periodized Haar wavelets (see § A.2). Let A_g consist of low frequency non-constant trigonometric polynomials. More precisely, for $L = 1, \dots, d/2 - 1$ consider the following families of real sinusoids

$$(10) \quad \begin{aligned} \chi_l^1(\alpha) &= c_l^1 \sin(2\pi l_1 \alpha_1/d) \sin(2\pi l_2 \alpha_2/d), & l_1, l_2 &= 1, \dots, L, \\ \chi_l^2(\alpha) &= c_l^2 \sin(2\pi l_1 \alpha_1/d) \cos(2\pi l_2 \alpha_2/d), & l_1 &= 1, \dots, L, l_2 = 0, \dots, L, \\ \chi_l^3(\alpha) &= c_l^3 \cos(2\pi l_1 \alpha_1/d) \sin(2\pi l_2 \alpha_2/d), & l_1 &= 0, \dots, L, l_2 = 1, \dots, L, \\ \chi_l^4(\alpha) &= c_l^4 \cos(2\pi l_1 \alpha_1/d) \cos(2\pi l_2 \alpha_2/d), & l &\in \{0, \dots, L\}^2 \setminus \{(0, 0)\}, \end{aligned}$$

where $c_l^i > 0$ are suitable normalization factors chosen so that $\|\chi_l^i\|_2 = 1$. Let A_g be the collection of all these real sinusoids. Assumption (4) is satisfied. The number of atoms is given by $m_g = 4L^2 + 4L$. The proof of the following result is given in Appendix A.2: it is heavily based on the structure of Haar wavelets, and so it is expected that this result would fail with smoother wavelets.

Proposition 3. *Let A_f and A_g be the dictionaries of 2D Haar wavelets and low frequency non-constant real sinusoids discussed above, respectively. Assume that $L < 2^B$ for some $B \leq J - 2$. There exists $D > 0$ such that*

$$\|q\|_0 \geq \sum_{j=1}^{J-B-1} (2^{J-j} - 2L)^2,$$

for every $q \in \mathbb{R}^n$ with $\|A_f q\|_2 > D$ and $\|{}^t A_g^\perp A_f q\|_2 \leq 2/3$.

Example 2. In Section 5 we shall set $J = 7$ and $L = 15$. In this case, the above inequality reads $\|q\|_0 \geq 1160$, which is sensibly better than the uncertainty principle based on the mutual coherence. Thus, arguing as in Remark 2, in the single-measurement case, condition CS2 is satisfied provided that

$$(11) \quad 2\|\tilde{y}_f\|_0 + \|\tilde{y}_g\|_0 < 1160.$$

It should be observed that in the numerical simulations we add also the constant matrix to the dictionary A_g . Even if this is not allowed by the above result (only 4 wavelets are needed to represent it), it seems not to create any issues for the reconstruction. This might be due to the following remark: most images are not constant.

Remark 3. We conclude this part by observing that these uncertainty principles always take into account the worst case scenarios; namely, for most vectors the minimum is not attained. Improved bounds (called *robust* uncertainty principles) that hold for the overwhelming majority of vectors were proved in [32] for spikes and sinusoids. Moreover, it was proven that the separation problem can be successfully solved in most cases by using l_0 minimization, provided that corresponding sparsity conditions are satisfied. These conditions are much weaker than the ones based on exact uncertainty principles. It would be interesting to investigate whether such extensions hold in our context too.

In view of this, while the uncertainty principle in Proposition 3 does not contain the term corresponding to S_q , it seems reasonable to assume that for most vectors the quantity $\#S_q$ is not small when $\|q\|_0$ is close to the minimum. This explains why CS2 is easily satisfied when N is bigger, at least for most q .

3.3. Main result. The main result of this section states that if the \tilde{y}_g^i 's constitute a complete set, then the signals \tilde{f} and \tilde{g}_i can be stably recovered from the knowledge of $h_i = \tilde{f} + \tilde{g}_i + n_i$ by minimizing (5).

Theorem 1. *Assume that (4) holds true. Let $\beta, D, \rho_f, \rho_g, \eta > 0$ and $N \in \mathbb{N}^*$ be such that $\varepsilon := \rho_f + \rho_g + \eta \leq \beta/3$. Take $\tilde{y}_f \in \mathbb{R}^{m_f}$ and let $\{\tilde{y}_g^1, \dots, \tilde{y}_g^N\}$ be (β, D) -complete. Assume that $\tilde{f}, \tilde{g}_i, n_i, h_i \in \mathbb{R}^n$ satisfy (6), (7) and (8) and let $y_f \in \mathbb{R}^{m_f}$ and $y_g^i \in \mathbb{R}^{m_g}$ realize the minimum of*

$$(12) \quad \min_{y \in \mathbb{R}^{m_f + Nm_g}} \|y\|_0 \quad \text{subject to } \|A_f y_f + A_g y_g^i - h_i\|_2 \leq \varepsilon, \quad i = 1, \dots, N.$$

Then for every $i = 1, \dots, N$

$$\|A_f y_f - \tilde{f}\|_2 \leq (3D + 1)\varepsilon, \quad \|A_g y_g^i - \tilde{g}_i\|_2 \leq (3D + 2)\varepsilon.$$

Thanks to this result, the reconstruction can be performed by minimizing (12) and then taking $\hat{f} \approx A_f y_f$ and $\hat{g}_i \approx A_g y_g^i$. The practical details of such minimization will be discussed in Section 4.

In the proof of this theorem we shall make use of the following properties, whose proofs are immediate.

Lemma 1. *Let $A \in \mathbb{R}^{n \times m}$ constitute an orthonormal set of \mathbb{R}^n and let $A^\perp \in \mathbb{R}^{n \times (n-m)}$ complete A to an orthobasis of \mathbb{R}^n . The following properties hold true.*

- (1) For every $v \in \mathbb{R}^m$ we have $\|Av\|_2 = \|v\|_2$.
- (2) For every $v \in \mathbb{R}^n$ we have $\|{}^tAv\|_2 \leq \|v\|_2$.
- (3) We have ${}^tAA = I$ and ${}^tA^\perp A = 0$.
- (4) For every $a, b \in \mathbb{R}^m$ we have

$$\|a + b\|_0 = \|a\|_0 + \#(\text{supp } b \setminus \text{supp } a) - \#\{\alpha : a(\alpha) = -b(\alpha) \neq 0\}.$$

We are now ready to prove Theorem 1.

Proof of Theorem 1. Write $f := A_f y_f$, $g_i := A_g y_g^i$, $e_f := y_f - \tilde{y}_f$, $e_g^i := y_g^i - \tilde{y}_g^i$, $e_g := -{}^tA_g A_f e_f$ and $r^i := e_g^i - e_g$. Since y_f and y_g^i satisfy the constraint in (12) we have

$$\begin{aligned} \|A_f y_f - A_f \tilde{y}_f + A_g y_g^i - A_g \tilde{y}_g^i\|_2 &\leq \|(A_f y_f + A_g y_g^i - h_i) + (h_i - A_g \tilde{y}_g^i - A_f \tilde{y}_f)\|_2 \\ &\leq \varepsilon + \|\tilde{f} - A_f \tilde{y}_f\|_2 + \|\tilde{g}_i - A_g \tilde{y}_g^i\|_2 + \|n_i\|_2 \\ &\leq 2\varepsilon \end{aligned}$$

where the last inequality follows from (7) and (8). As a consequence, since $r^i = {}^tA_g(A_f y_f - A_f \tilde{y}_f + A_g y_g^i - A_g \tilde{y}_g^i)$ (Lemma 1 part 3), by Lemma 1 part 2 we obtain $\|r^i\|_2 \leq 2\varepsilon$, whence

$$(13) \quad \|r^i\|_\infty \leq 2\varepsilon.$$

Moreover, by Lemma 1 parts 2 and 3 we obtain

$$(14) \quad \|{}^tA_g^\perp A_f e_f\|_2 = \|{}^tA_g^\perp (A_f y_f - A_f \tilde{y}_f + A_g y_g^i - A_g \tilde{y}_g^i)\|_2 \leq 2\varepsilon.$$

Since y_f and y_g^i realize the minimum of (12) we have $\|y\|_0 \leq \|\tilde{y}\|_0$ or, equivalently,

$$(\|y_f\|_0 - \|\tilde{y}_f\|_0) + \sum_{i=1}^N (\|y_g^i\|_0 - \|\tilde{y}_g^i\|_0) \leq 0.$$

where we have set $\tilde{y} = {}^t[\tilde{y}_f, \tilde{y}_g^1, \dots, \tilde{y}_g^N]$. Thus, since $y_f = \tilde{y}_f + e_f$ and $y_g^i = \tilde{y}_g^i + e_g^i$, Lemma 1 part 4 yields

$$(15) \quad \#(\text{supp } e_f \setminus \text{supp } \tilde{y}_f) - \#\{\alpha : \tilde{y}_f(\alpha) = -e_f(\alpha) \neq 0\} \\ + \sum_{i=1}^N \#(\text{supp } e_g^i \setminus \text{supp } \tilde{y}_g^i) - \sum_{i=1}^N \#\{\alpha : \tilde{y}_g^i(\alpha) = -e_g^i(\alpha) \neq 0\} \leq 0.$$

Observe now that by (13) we have

$$(16) \quad \#\{\alpha : \tilde{y}_f(\alpha) = -e_f(\alpha) \neq 0\} \leq \|\tilde{y}_f\|_0, \\ \text{supp } e_g^i = \text{supp } (e_g + r^i) \supseteq \{\alpha : |e_g(\alpha)| \geq 3\varepsilon\}.$$

Since $3\varepsilon \leq \beta$ and $\{\tilde{y}_g^1, \dots, \tilde{y}_g^N\}$ is (β, D) -complete, by (13) and Definition 1 (condition CS1), we have

$$(17) \quad \sum_{i=1}^N \#\{\alpha : \tilde{y}_g^i(\alpha) = -e_g^i(\alpha) \neq 0\} = \#\bigcup_{i=1}^N \{\alpha : \tilde{y}_g^i(\alpha) = -e_g^i(\alpha) \neq 0\} \leq \#\bigcup_{i=1}^N \text{supp } \tilde{y}_g^i.$$

Inserting (16) and (17) into (15) gives

$$\#(\text{supp } e_f \setminus \text{supp } \tilde{y}_f) + \sum_{i=1}^N \#\{\alpha : |({}^t A_g A_f e_f)(\alpha)| \geq 3\varepsilon\} \setminus \text{supp } \tilde{y}_g^i \leq \|\tilde{y}_f\|_0 + \#\bigcup_{i=1}^N \text{supp } \tilde{y}_g^i.$$

Set $q = e_f/(3\varepsilon)$. Since $\text{supp } e_f = \text{supp } q$ we have

$$\#(\text{supp } q \setminus \text{supp } \tilde{y}_f) + \sum_{i=1}^N \#(S_q \setminus \text{supp } \tilde{y}_g^i) \leq \|\tilde{y}_f\|_0 + \#\bigcup_{i=1}^N \text{supp } \tilde{y}_g^i.$$

where $S_q = \{\alpha : |({}^t A_g A_f q)(\alpha)| \geq 1\}$. Moreover, by (14) we have $\|{}^t A_g^\perp A_f q\|_2 \leq 2/3$. Thus, since $\{\tilde{y}_g^1, \dots, \tilde{y}_g^N\}$ is (β, D) -complete, by Definition 1 (condition CS2) we obtain that $\|A_f e_f\|_2 \leq 3D\varepsilon$. As a result, by construction of e_f , (8) and the triangle inequality we have

$$(18) \quad \|A_f y_f - \tilde{f}\|_2 \leq 3D\varepsilon + \rho_f \leq (3D + 1)\varepsilon.$$

This proves the desired bound for f . It remains to prove the corresponding estimate for $g_i = A_g y_g^i$. In order to do this, observe that by (8), (18) and the triangle inequality we obtain

$$\|g_i - \tilde{g}_i\|_2 \leq \|(f + g_i - h_i) + (\tilde{f} - f) + n_i\|_2 \leq \varepsilon + 3D\varepsilon + \rho_f + \eta \leq (3D + 2)\varepsilon.$$

This concludes the proof. \square

4. NUMERICAL IMPLEMENTATION

4.1. Orthogonal Matching Pursuit. The simplest available algorithm for the minimization of problems of the type

$$\min_{y \in \mathbb{R}^m} \|y\|_0 \quad \text{subject to } \|Ay - f\|_2 \leq \varepsilon,$$

for $f \in \mathbb{R}^n$ and $A \in \mathbb{R}^{n \times m}$, is the Orthogonal Matching Pursuit (OMP) [59, 27]. This algorithm belongs to a wider class of methods called greedy algorithms, in which the set of the used atoms of A is increased step by step. In OMP, the best coefficients for the atoms are recomputed at each iteration, which makes it more efficient compared to the standard matching pursuit. Greedy algorithms, and hence OMP, are not a priori equivalent to the minimization of the above problem, and the convergence to a minimizer is not always guaranteed, but they have been proved to perform well in most cases [72]. The reader is referred to [27] for more details on this topic.

The adaptation of OMP to the problem of our interest is quite straightforward. By Theorem 1, we need to minimize (12), i.e.

$$\min_{y \in \mathbb{R}^{m_f + Nm_g}} \|y\|_0 \quad \text{subject to } \|A_f y_f + A_g y_g^i - h_i\|_2 \leq \varepsilon, \quad i = 1, \dots, N,$$

given N signals $h_i \in \mathbb{R}^n$ and two dictionaries $A_f \in \mathbb{R}^{n \times m_f}$ and $A_g \in \mathbb{R}^{n \times m_g}$. Setting

$$A = \begin{bmatrix} A_f & A_g & 0 & \cdots & 0 \\ A_f & 0 & A_g & \ddots & \vdots \\ \vdots & \vdots & \ddots & \ddots & 0 \\ A_f & 0 & \cdots & 0 & A_g \end{bmatrix}, \quad y = \begin{bmatrix} y_f \\ y_g^1 \\ y_g^2 \\ \vdots \\ y_g^N \end{bmatrix} \quad \text{and} \quad h = \begin{bmatrix} h_1 \\ h_2 \\ \vdots \\ h_N \end{bmatrix},$$

the above problem is equivalent to

$$\min_{y \in \mathbb{R}^{m_f + Nm_g}} \|y\|_0 \quad \text{subject to } \|Ay - h\|_2 \leq \sqrt{N}\varepsilon,$$

for which the OMP can be applied directly, as discussed above. As before, OMP is not guaranteed to converge to a minimizer of this functional. In other words, even though Theorem 1 gives (almost) exact recovery via the minimization of (12), OMP may not provide a faithful reconstruction. However, the numerical simulations (Section 4) suggest that in practice a correct reconstruction is always achieved via OMP. It would be interesting to consider this issue from the theoretical point of view, but this goes beyond the scope of this work.

Let us also mention other alternatives for the minimization of these problems, such as Basis Pursuit [36], Block-Coordinate-Relaxation [26], Iterative Hard Thresholding [22] and Stagewise OMP [43]. In particular, in Basis Pursuit the ℓ^0 -penalization term is substituted by an ℓ^1 term, which makes the functional convex: the minimization can be easily achieved with standard tools. This would complicate the corresponding reconstruction result (Theorem 1) and consequently the assumptions on the original signals (Definition 1). Achieving this would be a natural follow-up of this work.

The Block-Coordinate-Relaxation method was adapted to the minimization of the functional related to the separation problem with $N = 1$ measurement [69]. This method, sometimes referred as MCA, is a combination of Basis Pursuit (the

ℓ^1 norm is used instead of the ℓ^0 norm) and of a two-step iterative procedure where the two components of the signal are minimized separately. Moreover, the minimization is expressed directly in terms of the signals $A_f y_f$ and $A_g y_g$, without the need of storing the full dictionary matrices, which may take a lot of memory space. It would be very interesting to see whether this method can be generalized to the multi-measurement case considered in this paper.

4.2. Dictionaries for image content. Let us now discuss what choices may be done for the dictionaries A_f and A_g in the context we are interested in, namely hybrid imaging inverse problems. As we shall see in Section 5, in such problems the signal \tilde{f} will typically represent (the logarithm of) a constitutive parameter of the tissue under investigation, like for instance the electric permittivity, electric conductivity or the optical absorption. As such, the image \tilde{f} can be supposed to be piecewise smooth: the discontinuities are usually the inclusions we would like to determine. On the other hand, the signals \tilde{g}_i 's usually represent the injected fields, such as the electric field or the light intensity, and are the solutions to certain PDE. As such, they enjoy higher regularity properties, and the images \tilde{g}_i 's can be supposed to be smooth.

These different features represent the foundation of the signal separation method discussed in the previous section. In order to exploit this diversity it is necessary to choose suitable dictionaries A_f and A_g , with respect to which \tilde{f} and the \tilde{g}_i 's have sparse representations, respectively.

As far as A_f is concerned, wavelets have been widely used to sparsely represent piecewise smooth images [70]. In particular, Haar wavelets will be used in this work: the choice is motivated by Proposition 3. It is worth noting that in recent years a large number of new multi-dimensional transforms have been introduced in order to capture the directional features of two-dimensional images [65]. Among the most known, there are curvelets [30], ridgelets [29] and shearlets [58, 57, 52]. The use of these transforms may give better results, but a deep investigation of the best choice for the dictionaries goes beyond the scope of this paper. Thus, we have decided to make the most classical choice of wavelets, since, even though possibly not optimal, it is sufficient to properly illustrate the disjoint sparsity signal separation method.

The situation is simpler for the choice of A_g . Indeed, a good representation of smooth functions may be obtained by choosing low frequency trigonometric polynomials. This is a simple consequence of the correspondence between the smoothness of a function and the decay of its Fourier transform. This represents our choice for A_g in this paper.

These dictionaries purely represent a general guideline for the choices of A_f and A_g . Additional information on the particular physical model may be used to select dictionaries more adapted to the features of the images under consideration.

5. APPLICATIONS TO HYBRID INVERSE PROBLEMS

5.1. Introduction. We have seen in the introduction that a hybrid problem usually involves two steps. First, internal functionals are measured inside the domain and, second, from their knowledge the unknown coefficients of the PDE have to be reconstructed. These internal data are linear or quadratic functionals of the unknowns and of the solutions of the direct problem. Let us mention some examples.

- In photoacoustic tomography [11, 12, 21, 19] the internal data take the form

$$H(x) = \Gamma(x)\mu(x)u(x), \quad x \in \Omega,$$

where Γ is the Grüneisen parameter, μ is the optical absorption and u is the light intensity. The main unknown of the problem is μ . The photoacoustic image H gives only qualitative information on the medium, as μ is multiplied by Γ and u . The problem of quantitative photoacoustics is the reconstruction of μ from H . Under the diffusion approximation, the light intensity u solves

$$(19) \quad -\operatorname{div}(D\nabla u) + \mu u = 0 \quad \text{in } \Omega,$$

where D is the diffusion parameter. This equation should be augmented with suitable boundary conditions, such as of Dirichlet or Robin type.

- In thermoacoustic tomography [14] the internal data take the form

$$H(x) = \sigma(x)|u(x)|^2, \quad x \in \Omega,$$

where σ is the unknown conductivity and u is the electric field. The problem of quantitative thermoacoustics is the reconstruction of σ from H . In the scalar approximation, u is the solution of the Helmholtz equation

$$\Delta u + (\omega^2 + i\omega\sigma)u = 0 \quad \text{in } \Omega,$$

where ω is the angular frequency. As before, this equation should be augmented with suitable boundary conditions.

- In microwave imaging by ultrasound deformation [13, 1] the internal data take the form

$$H(x) = \varepsilon(x)u(x)^2, \quad x \in \Omega,$$

where ε is the unknown electric permittivity and u is the electric field. The problem is now to reconstruct ε from H . In the scalar approximation, u is the solution of the Helmholtz equation

$$\Delta u + \omega^2\varepsilon u = 0 \quad \text{in } \Omega,$$

augmented with suitable boundary conditions.

- In ultrasound modulated diffuse optical tomography [10, 9, 15] the internal data are $\operatorname{div}(u^2\nabla\mu)$, where u solves (19) and μ is the optical absorption.

In all the above examples, the measurement H is the product of the desired unknown and other quantities. Thus, the problem is extracting the desired unknown from H . PDE techniques are usually used to solve the problem, but, as discussed in the introduction, have several drawbacks.

All the above problems consist in the determination of two functions from the knowledge of their product. Taking logarithms, in a multi-measurement setting this is equivalent to finding $f(x)$ and $g_i(x)$ from the knowledge of their sums

$$h(x) = f(x) + g_i(x), \quad x \in \Omega.$$

The disjoint sparsity signal separation method can be applied since f and the g_i 's have different level of smoothness, and so can be sparsely represented with respect to different dictionaries (see § 4.2).

In particular, Theorem 1 guarantees unique and stable reconstruction of the the coefficients, provided that we can construct many incoherent u_i of the above problems (by changing the boundary values), so that the corresponding g_i 's give a complete set of measurements, according to Definition 1. As we shall see below in the numerical simulations, the conclusion of Theorem 1 is verified in several cases,

choosing different boundary values. Unfortunately, it is not possible to check the conditions of Definition 1 numerically, as this would require an infinite number of computations. These conditions are used to heuristically inform the choice of incoherent illuminations. On the other hand, at the current state, we are unable to give a general strategy to build boundary values so that the corresponding solutions will satisfy the hypotheses of Definition 1: this represents a very interesting open problem regarding the interplay of the PDE theory with the disjoint sparsity approach (see Section 6).

It is worth mentioning that similar assumptions of incoherence, usually in terms of linear independence of gradients of solutions, are often necessary for the PDE-based reconstruction methods (see, e.g., [33, 21, 13, 14, 1, 17, 2, 3, 61] and references therein).

As an example, in the rest of this section we shall apply the method to the reconstruction in quantitative photoacoustic tomography. All the other modalities mentioned above can be treated with minor modifications.

5.2. Quantitative photoacoustic tomography, the case $\Gamma = 1$. In photoacoustic tomography, the object under investigation is illuminated with light radiation, whose absorption causes local heating of the medium. The temperature rise creates an expansion of the tissue, thereby producing an acoustic wave, that can be measured on the boundary of the domain. The first step of this hybrid modality consists in the recovery of the amount of absorbed radiation by inverting the wave equation, from the knowledge of the boundary values. This problem has attracted much attention in the last years: the reader is referred to [54] and to the references therein for more details. In this paper, we shall suppose that the first step has been performed, and that we have access to the amount of absorbed radiation

$$H(x) = \Gamma(x)\mu(x)u(x), \quad x \in \Omega,$$

where Γ is the Grüneisen parameter, μ is the optical absorption and u is the light intensity. The problem of quantitative photoacoustic tomography consists in the reconstruction of μ from the knowledge of H . Much research has been done on this over the last years, see e.g. [39, 64, 40, 11, 38, 68, 49, 63, 62] and references therein. Sparse representations were first used in [64]. Recently, one-step methods have been introduced to perform both steps at the same time [51, 41]: it would certainly be interesting to see whether the signal separation approach can be employed in a one-step reconstruction method.

Light propagation may be modeled by a radiative transport equation or, when the scattering coefficient is large and the absorption is small, by its diffusion approximation (19). We consider here the simplest case when $\Gamma = 1$, the general case is discussed later in § 5.3. By using multiple measurements, μ can be recovered both in the transport regime [18] and in the diffusive regime [21], under suitable assumptions on the solutions.

We now describe how to apply the disjoint sparsity approach to this problem. If compared to the PDE approach, the separation of μ and u does not require the use of a PDE, and so no specific model of light propagation has to be assumed for the inverse problem. Moreover, no a priori knowledge of relevant boundary conditions (which may be unrealistic) is required, in contrast to the PDE approach. These aspects should make this approach more feasible. For simplicity, we shall construct

the solutions u_i via (19) with $D = 1$ and Dirichlet boundary values, namely

$$(20) \quad \begin{cases} -\Delta u_i + \mu u_i = 0 & \text{in } \Omega, \\ u_i = \varphi_i & \text{on } \partial\Omega. \end{cases}$$

However, this equation will not be used for the inversion.

The joint sparsity method will be applied as follows. Let $\tilde{\mu}$ denote the true absorption. After constructing N solutions $\tilde{u}_1, \dots, \tilde{u}_N$ to the above equation, the quantities

$$H_i(x) = \tilde{\mu}(x)\tilde{u}_i(x), \quad x \in \Omega,$$

are measured. Taking logarithms and adding white Gaussian noise n_i , we obtain

$$(21) \quad h_i = \log \tilde{\mu} + \log \tilde{u}_i + n_i, \quad i = 1, \dots, N.$$

The reconstruction of $\tilde{\mu}$ from the knowledge of the h_i 's exactly corresponds to the problem discussed in Section 3. The method based on Theorem 1 and whose numerical implementation is described in Section 4 will be used for the reconstruction.

In all the examples, we shall consider the two-dimensional domain $[0, 1]^2$ with 128×128 pixels. As far as the choice for the dictionaries is concerned, we let A_f consist of the orthonormal basis of Haar wavelets (as in § A.2) and let A_g consist of 961 low frequency trigonometric polynomials (as in (10), including the constant matrix), periodic over $[0, 1]^2$.

The choice for A_g forces to choose periodic boundary conditions, and so we set

$$(22) \quad \begin{aligned} \varphi_1(x) &= 1, \\ \varphi_2(x) &= 1 - \sin(2\pi x_1)/4, \\ \varphi_3(x) &= 1 - \sin(2\pi x_2)/4, \\ \varphi_4(x) &= 1 - \cos(2\pi x_2)/4, \\ \varphi_5(x) &= 1 - \cos(2\pi x_1)/4. \end{aligned}$$

(For physical constraints, all the quantities have to be positive.) Non-periodic choices for the boundary conditions would be allowed with no added difficulties for the reconstruction, provided that the dictionary A_g is properly chosen. The above boundary values are expected to generate incoherent solutions to (20) in such a way to satisfy the conditions of complete sets as in Definition 1. In this case, the assumptions of Theorem 1 would be verified and the disjoint sparsity separation method would be guaranteed to provide the right reconstruction, even in presence of noise. However, this is not guaranteed a priori: as mentioned above, the conditions of Definition 1 are very hard to check.

5.2.1. Example 1 - convex inclusions. We consider three convex constant inclusions in a homogeneous background, as shown in Figure 1a. We choose to stop the iteration procedure of OMP after 1500 iterations, which gives satisfactory results. More accurate stopping criteria may be considered [64], but this is not among the aims of this work.

In a first experiment we consider one noise-free measurement, namely we set $N = 1$ and $n_1 = 0$ in (21). The results are shown in Figure 1. The solution to (20) with boundary value $\varphi_1 = 1$ is shown in Figure 1b, and the corresponding measurement $H_1 = \tilde{\mu}\tilde{u}_1$ in Figure 1c. As it is evident from the images, the inclusions are still clearly recognizable in H_1 , but the corresponding values of the absorption are corrupted by the multiplication by \tilde{u}_1 . The sparse separation approach is thus

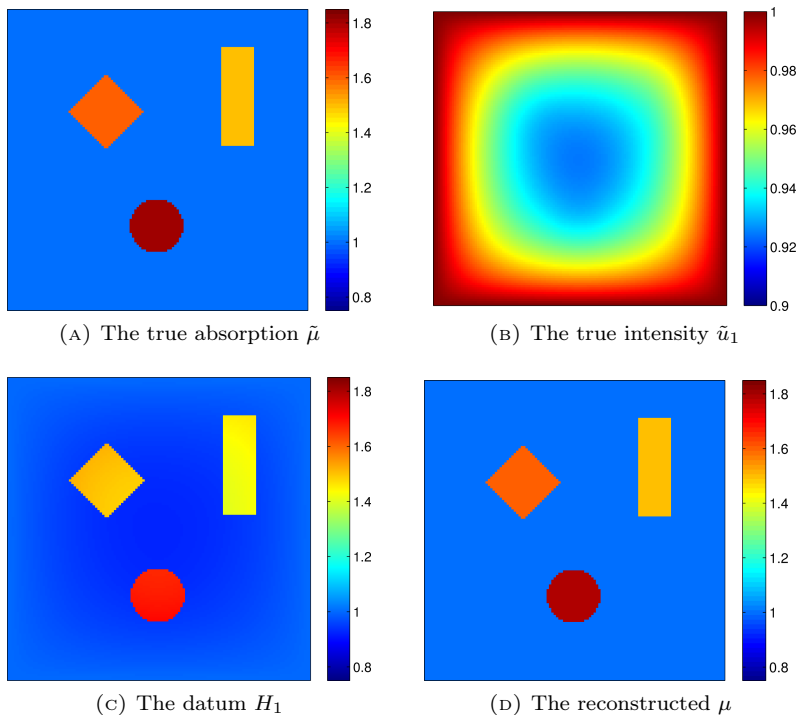


FIGURE 1. Example 1. Noise-free case with one measurement.

applied as discussed above, and the reconstructed μ is shown in Figure 1d. The relative reconstruction error is

$$\frac{\|\log \mu - \log \tilde{\mu}\|_2}{\|\log \tilde{\mu}\|_2} \approx 1.5\%.$$

This shows that, in absence of noise, the reconstruction is almost exact, even with only one measurement. This is in total agreement with the theoretical result discussed above. In the absence of noise ($\eta = 0$), it is possible to satisfy the conditions in Definition 1 in view of Proposition 3 and Example 2. Indeed, the sparse approximations of $\log \tilde{\mu}$ and of $\log \tilde{u}_1$ with 500 wavelets and 100 sinusoids, respectively, give small approximation errors, namely $\rho_f \approx 0.54$ and $\rho_g \approx 0.05$. By (11), CS2 is satisfied. Thus, the assumptions of Theorem 1 are verified with $\varepsilon \approx 0.59$, and the resulting reconstruction is very good ($\|\log \mu - \log \tilde{\mu}\|_2 \approx 0.29$). As already mentioned in Example 2, this argument is not fully rigorous, since Proposition 3 does not allow the constant image to be in the dictionary A_g .

In a second experiment (Figure 2) we add white Gaussian noise n_i in (21). The noise level is so that

$$\frac{\|n_i\|_2}{\|\log(\tilde{\mu}\tilde{u}_i)\|_2} \approx 17.6\%.$$

We tested the reconstruction procedure for $N = 1, \dots, 5$ and the boundary values φ_i as in (22). The data H_i , $i = 1, 3, 5$, are shown in Figures 2a, 2c and 2e, respectively. The reconstructed μ 's for $N = 1$, $N = 3$ and $N = 5$ are shown in Figures 2b, 2d and 2f, respectively. The reconstruction errors for $N = 1, \dots, 5$ are given in Table 1.

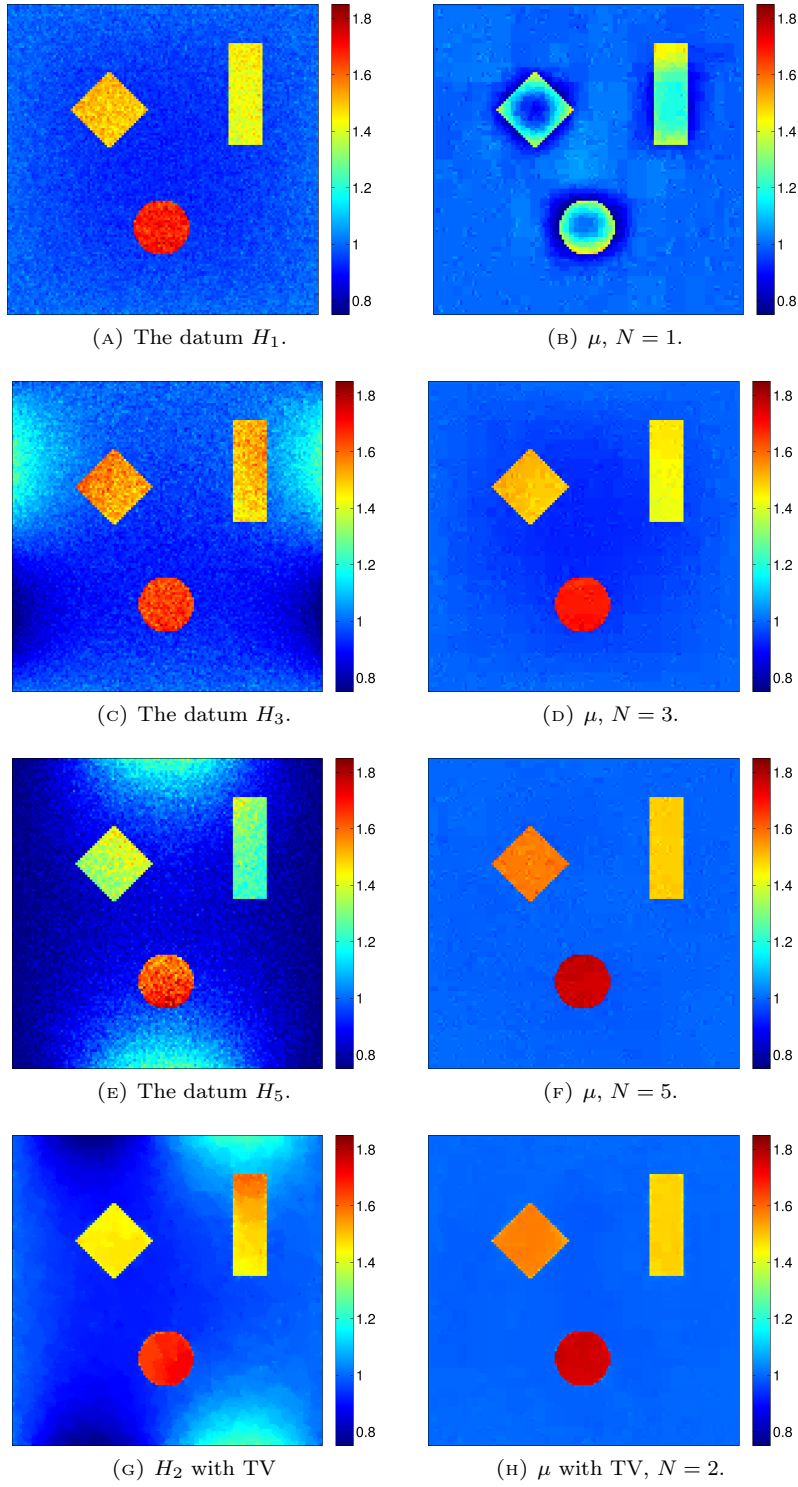


FIGURE 2. Example 1. Noisy case with multiple measurements.

TABLE 1. Example 1. The reconstruction errors $\|\log \mu - \log \tilde{\mu}\|_2 / \|\log \tilde{\mu}\|_2$ for the noisy data.

N	1	2	3	4	5
No regularization	74.4%	32.2%	28.4%	15.8%	7.5%
TV regularization	23.2%	6.0%	22.1%	4.8%	4.6%

It is evident that the larger N is, the more accurate the reconstruction becomes. More precisely, when $N = 1$ the reconstructed values of the absorption in the inclusions are completely wrong. This is due to the fact that the inclusions are roughly approximated by smooth atoms in A_g and then corrected with fewer atoms in A_f , and so the sparsest approximation does not separate the two components as desired. Choosing the same sparse approximations discussed above (so that CS2 is satisfied with $N = 1$) gives a big value for ε in the noisy case, and so the reconstruction is not accurate. However, the problem is solved when more measurements are added: CS2 is easily satisfied with lower values of ρ_f and ρ_g when N becomes bigger (see Remark 1).

The reconstruction with $N = 5$ is very satisfactory if measurement and reconstruction errors are compared. Indeed, the noise from the data has almost disappeared in the reconstruction, without a separate regularization. This is due to the implicit regularizing effect that sparse representations provide.

We have also investigate the effect of an a priori total variation (TV) regularization [66] of the measurements h_i on the reconstruction, using a Matlab implementation based on the algorithm developed in [34]. The regularization parameter was chosen a posteriori to achieve the best results, but in principle it can be learned from a training set [28]. The corresponding reconstruction errors with different values of N are shown in Table 1: the improvement is significant only for a low number of measurements. For comparison, the regularized value of H_2 is shown in Figure 2g (where the usual staircase effect can be observed) and the reconstruction with $N = 2$ measurements is shown in Figure 2h.

5.2.2. *Example 2 - The Shepp-Logan phantom.* Here, we let $\tilde{\mu}$ be the well-known Shepp-Logan phantom (shown in Figure 3a). We choose to stop the iterative procedure of OMP after 2000 iterations. As above, we consider the boundary conditions φ_i as in (22) and the corresponding solutions \tilde{u}_i to (20), for $i = 1, \dots, 5$, and measure the quantities h_i as in (21).

TABLE 2. Example 2. Reconstruction errors for the noise-free case.

N	1	2	3	4	5
$\ \log \mu - \log \tilde{\mu}\ _2 / \ \log \tilde{\mu}\ _2$	68.6%	24.8%	18.6%	11.4%	5.4%

In a first experiment we consider the case without noise (Figure 3). The reconstruction errors for $N = 1, \dots, 5$ are shown in Table 2. We see that the reconstruction quality improves as N increases, as it is expected from the general theory discussed in Section 3. From a comparison with the previous case without noise, we notice that more measurements are needed to have a satisfactory reconstruction. This is due to the more complicated structure of the phantom, which has a

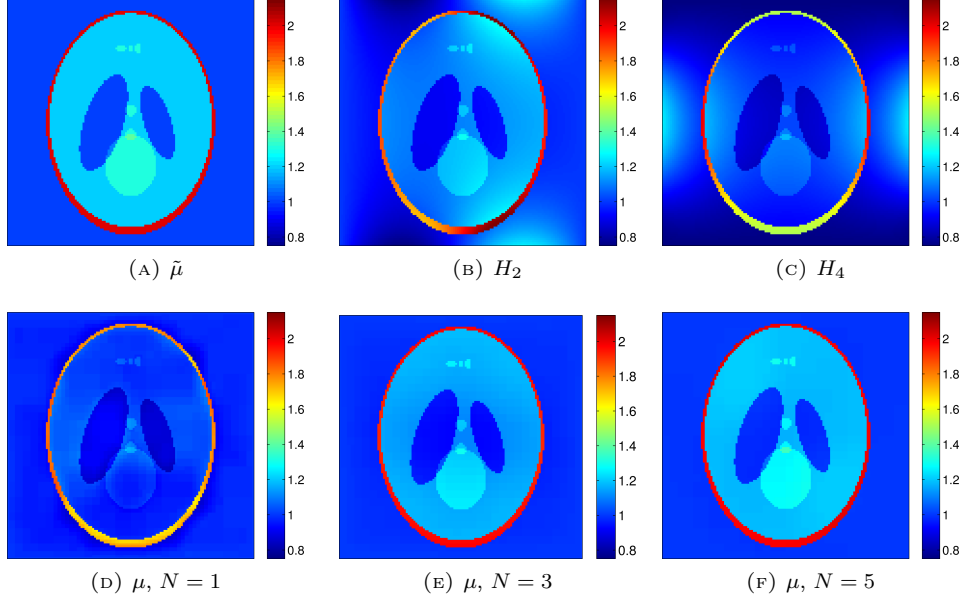
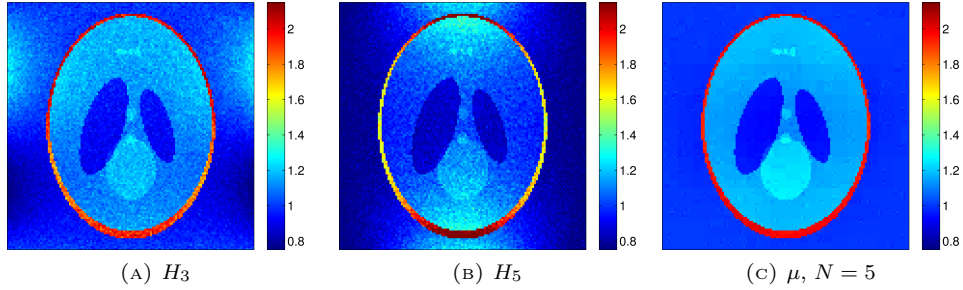


FIGURE 3. Example 2. Noise-free case with multiple measurements.

FIGURE 4. Example 2. Noisy case with $N = 5$ measurements.

less sparse representation in terms of Haar wavelets than the absorption considered in the previous case. Thus, a higher N is needed to satisfy the conditions in Definition 1.

In a second experiment we add white Gaussian noise n_i to the data in (21). The noise level is such that

$$\frac{\|n_i\|_2}{\|\log(\tilde{\mu}\tilde{u}_i)\|_2} \approx 17.8\%.$$

Motivated by the noisy-free case, we perform the reconstruction with $N = 5$ measurements. The reconstruction error is $\|\log \mu - \log \tilde{\mu}\|_2 / \|\log \tilde{\mu}\|_2 = 17.0\%$, that is comparable to the measurement error. The results are shown in Figure 4. It is expected that adding more measurements would improve the quality of the reconstruction.

5.3. Quantitative photo-acoustic tomography in the diffusive regime with variable Γ .

5.3.1. *Introduction.* We consider here the problem of quantitative photoacoustic tomography, as introduced above, without the further assumption $\Gamma = 1$. Thus, the unknown absorption μ has to be reconstructed from

$$H(x) = \Gamma(x)\mu(x)u(x), \quad x \in \Omega.$$

We consider the diffusion approximation (19) of light propagation:

$$(23) \quad -\operatorname{div}(D\nabla u) + \mu u = 0 \quad \text{in } \Omega.$$

For simplicity, here we shall augment this equation with Dirichlet boundary conditions, that are supposed to be measurable. Note that D , Γ and μ are unknowns of the problem. In contrast with the case $\Gamma = 1$, where (23) was merely used to compute the data but not in the inverse problem, we shall make full use of this PDE. Let us briefly review the main known results on this inverse problem. Bal and Ren [19] showed that when Γ , D and μ are all unknown, then there is no uniqueness for the inverse problem even with all the measurements H for all solutions u to (23); namely, the PDE approach alone is not sufficient to reconstruct all the parameters. If any of these parameters is known, then the others may be reconstructed by using the PDE. The same authors have proved that all the coefficients may be uniquely reconstructed by using multi-frequency measurements, under certain assumptions on the dependency of the parameters on the frequency [20]. Naetar and Scherzer [61] studied the case of piecewise constant parameters: all the unknowns can be uniquely determined, but the method may be very sensitive to noise.

We propose here for the single-frequency case a mixed approach combining the following aspects.

- As in [19], the PDE (23) can be used in the reconstruction. However, one degree of freedom for the parameters remain.
- As in [61], the PDE method gives unique reconstruction under the finite dimensionality assumption of the coefficient spaces.
- The disjoint sparsity signal separation method may be applied to this case as in § 5.2.

The combination of such approaches consists in substituting the piecewise constant assumption with the sparsity assumption, and then in the use of (23) to reconstruct all the parameters. More precisely, the reconstruction algorithm proposed here is substantially divided into the following three main steps.

- (1) By using the disjoint sparsity signal separation method applied to

$$h_i = \log H_i = \log(\Gamma\mu) + \log u_i, \quad i = 1, \dots, N,$$

the solutions u_i are reconstructed.

- (2) Following [19], by using the PDE

$$-\operatorname{div}(Du_i \nabla \frac{u_j}{u_i}) = 0 \quad \text{in } \Omega,$$

with three suitable measurements, the diffusion D can be uniquely determined.

- (3) Finally, the absorption can be directly reconstructed via

$$\mu = \frac{\operatorname{div}(D\nabla u_i)}{u_i} \quad \text{in } \Omega,$$

and possibly averaging over i .

5.3.2. *The reconstruction algorithm.* Even though theoretically satisfactory, the algorithm summarized above is not applicable in practice as it stands. Indeed, the reconstruction of D in (2) is not too sensitive to errors in u_j , but that of μ in (3) is. To understand this, we compare the solutions u_i to (23) with $D = 1$ and μ as in Figure 1a and the solutions u_i^0 to (23) with $D = 1$ and $\mu = \mu^0 = 1$, with boundary conditions given by (22):

$$(24) \quad \begin{cases} -\operatorname{div}(D\nabla u_i) + \mu u_i = 0 & \text{in } \Omega, \\ -\operatorname{div}(D\nabla u_i^0) + \mu^0 u_i^0 = 0 & \text{in } \Omega, \\ u_i = u_i^0 = \varphi_i & \text{on } \partial\Omega. \end{cases}$$

The solutions are shown in Figure 5. Looking at the first two columns, it is clear that the variations between u_i and u_i^0 are minimal. This is due to the fact that the two problems have the same diffusion coefficients and small variations in the absorption coefficients. As we saw in § 5.2, the reconstruction at step (1) cannot be at this level of precision, and therefore μ cannot be reconstructed in this simple way. In order to overcome this difficulty, we make the following observation.

Remark 4. The ratios u_i/u_i^0 are almost independent of i , provided that μ is a small variation around a known background μ^0 . This is evident from the third column of Figure 5, and can be proved by arguing as follows. A direct calculation gives that $v_i = u_i/u_i^0$ satisfies

$$\begin{cases} -\operatorname{div}(D\nabla v_i) + (\mu - \mu^0)v_i = 2\frac{\nabla u_i^0}{u_i^0} \cdot \left(\frac{\nabla u_i}{u_i} - \frac{\nabla u_i^0}{u_i^0}\right) & \text{in } \Omega, \\ v_i = 1 & \text{on } \partial\Omega. \end{cases}$$

When μ is close to μ^0 , the right-hand side of this equation becomes negligible with respect to the other terms. Thus, v_i is substantially independent of i .

Let us now describe the precise reconstruction algorithm based on these observations. It consists of two initial steps and an iterative procedure consisting of three more substeps. For simplicity, we shall discuss only the noise-free case. We suppose that μ is a small perturbation around a known coefficient μ^0 and that D is known at one point of the domain.

- (1) By using the disjoint sparsity signal separation method applied to

$$h_i = \log(\Gamma\mu) + \log u_i, \quad i = 1, \dots, N,$$

a first approximation $u_i(0)$ of the solutions u_i is reconstructed. As discussed in Section 4, this can be done by minimizing

$$\min_{y \in \mathbb{R}^{m_f + Nm_g}} \|y\|_0 + \lambda \sum_{i=1}^N \|A_f y_f + A_g y_g^i - h_i\|_2$$

with OMP, and then writing $u_i(0) = \exp(A_g y_g^i)$.

- (2) By using the computed $u_i(0)$ and the PDE

$$(25) \quad -\operatorname{div}(D u_i \nabla \frac{u_j}{u_i}) = 0 \quad \text{in } \Omega$$

with three suitable measurements, a first approximation $D(0)$ of the diffusion can be obtained. Indeed, choose three boundary values φ_1, φ_2 and φ_3 such

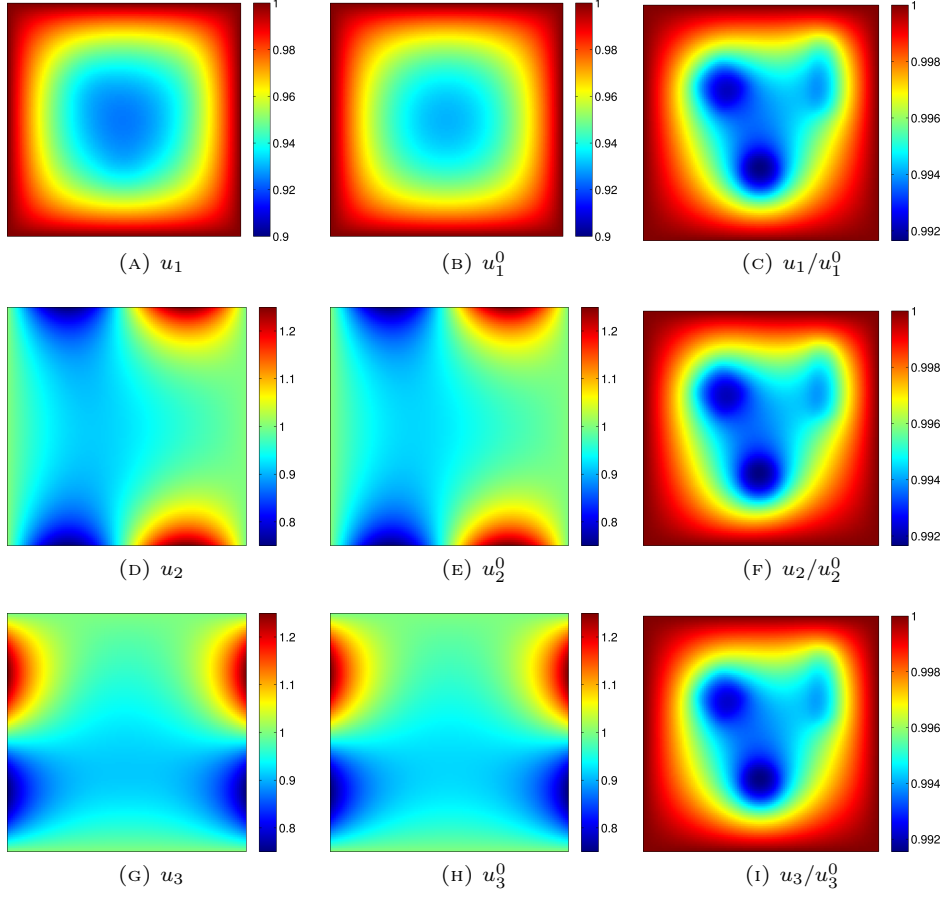


FIGURE 5. The solutions to 24 and their ratios.

that

$$(26) \quad \det\left(\nabla \frac{u_2}{u_1}, \nabla \frac{u_3}{u_1}\right) > 0, \quad \text{in } \Omega.$$

(This can be easily done in two dimensions [19].) Then the above PDE may be rewritten as

$${}^t(\nabla \log D) = - \left[\operatorname{div}(u_1 \nabla \frac{u_2}{u_1})/u_2 \quad \operatorname{div}(u_1 \nabla \frac{u_3}{u_1})/u_3 \right] \left[\nabla \frac{u_2}{u_1} \quad \nabla \frac{u_3}{u_1} \right]^{-1} \quad \text{in } \Omega,$$

which can be integrated over Ω and gives a unique solution for the diffusion coefficient, since D is known at one point of the domain. Since the solutions u_i are very sensitive to changes in D , we expect this reconstruction to be satisfactory. From the numerical point of view, an optimal control approach may be applied to (25) to find D .

- (3) We now start the main iterative procedure. Initialize $\mu(0) = \mu^0$ and let $u_i(0)$ and $D(0)$ be as reconstructed in points (1) and (2). From $\mu(k)$, $u_i(k)$ and $D(k)$, the following iteration is computed as follows.

(a) Given $D(k)$ and $\mu(k)$, let $u_i^0(k)$ be the unique solution to

$$\begin{cases} -\operatorname{div}(D(k)\nabla u_i^0(k)) + \mu(k)u_i^0(k) = 0 & \text{in } \Omega, \\ u_i^0(k) = \varphi_i & \text{on } \partial\Omega. \end{cases}$$

Since φ_i is known, $u_i^0(k)$ is a known datum. Therefore we can measure

$$h_i^0 = \log(H_i/u_i^0(k)) = \log(\Gamma\mu) + \log \frac{u_i}{u_i^0(k)}, \quad i = 1, \dots, N.$$

In view of Remark 4, the quantities $u_i/u_i^0(k)$ are almost independent of i . This leads to the minimization of

$$\begin{aligned} \min_{y \in \mathbb{R}^{m_f + (N+1)m_g}} \|y\|_0 + \lambda_1 \sum_{i=1}^N \|A_f y_f + A_g y_g^i - h_i\|_2 \\ + \lambda_2 \sum_{i=1}^N \|A_f y_f + A_g y_g^{N+1} - h_i^0\|_2 \end{aligned}$$

with $\lambda_1 \ll \lambda_2$. The second term maintains the incoherence among the y_g^i 's, on which this disjoint sparsity approach is based. The third term forces the quantities $u_i/u_i^0(k)$ to be independent of i , and numerical evidence shows that this gives a much better reconstruction than the one performed at point (1). The multipliers λ_1 and λ_2 may be taken dependent on k . Set $u_i(k+1) = u_i^0(k) \exp(A_g y_g^{N+1})$.

- (b) Given $u_i(k+1)$, find a better approximation $D(k+1)$ of the diffusion coefficient by proceeding as in (2).
(c) Reconstruct $\mu(k+1)$ via

$$(27) \quad \mu(k+1) = \frac{1}{N} \sum_{i=1}^N \frac{\operatorname{div}(D(k+1)\nabla u_i(k+1))}{u_i(k+1)} \quad \text{in } \Omega.$$

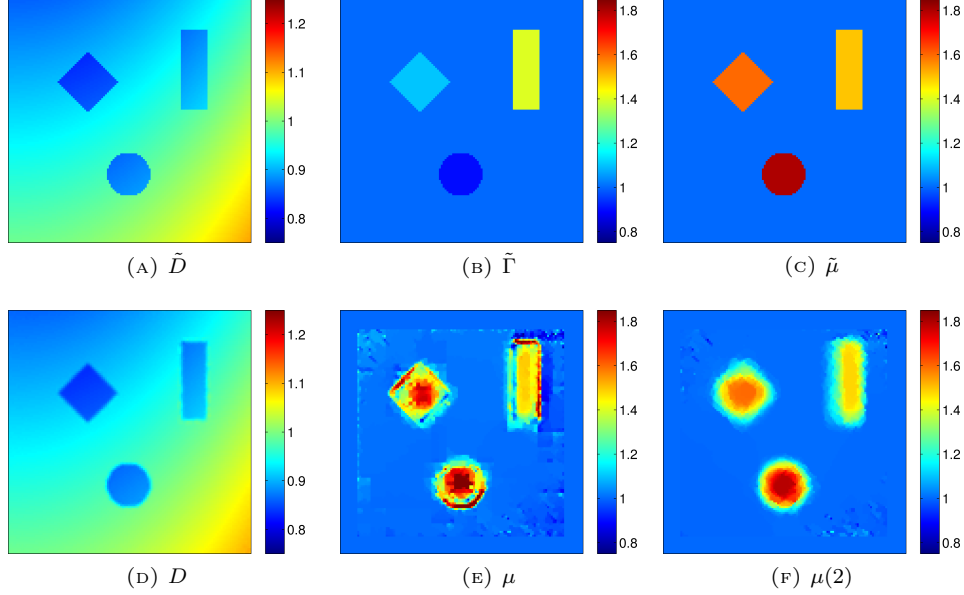
From the numerical point of view, it may be useful to regularize $u_i(k+1)$ and $D(k+1)$ before taking the derivatives. Finally, a TV-regularization of $\mu(k+1)$ may reduce the accumulated noise.

There is no obvious stopping criterion for this iterative procedure. However, in the numerical simulations less than five iterations were sufficient.

In the above algorithm we have assumed for simplicity that the boundary values φ_i are measurable. However, this is probably not a necessary conditions, since they may be obtained from point (1) as $\varphi_i = u_i(0)|_{\partial\Omega}$.

5.3.3. *Numerical simulations.* We have tested the algorithm discussed above with the absorption map $\tilde{\mu}$ considered in § 5.2.1 (see Figure 6c). The same dictionaries considered in § 5.2 are chosen. The light intensities \tilde{u}_i are the solutions of

$$\begin{cases} -\operatorname{div}(\tilde{D}\nabla \tilde{u}_i) + \tilde{\mu}\tilde{u}_i = 0 & \text{in } \Omega, \\ \tilde{u}_i = \varphi_i & \text{on } \partial\Omega, \end{cases}$$

FIGURE 6. The case with variable Γ .

where the diffusion coefficient \tilde{D} is shown in Figure 6a and five boundary values are chosen as follows:

$$\begin{aligned}\varphi_1(x) &= 1, \\ \varphi_2(x) &= 1 - \sin(2\pi x_1)/8, \\ \varphi_3(x) &= 1 - \sin(2\pi x_2)/8, \\ \varphi_4(x) &= x_1/4 + 7/8, \\ \varphi_5(x) &= x_2/4 + 7/8.\end{aligned}$$

The internal data take the form

$$H_i = \tilde{\Gamma}\tilde{\mu}\tilde{u}_i, \quad i = 1, \dots, 5,$$

where the Grüneisen parameter is shown in Figure 6b. The measurements corresponding to the first three boundary conditions will be used for the disjoint sparsity signal separation method (with $N = 3$), namely for the steps (1) and (3a) of the above algorithm; those corresponding to φ_1 , φ_4 and φ_5 will be used in the steps (2) and (3b), in order to satisfy (26). All measurements are used in the last step (3c).

The OMP iterative procedures are stopped after 2000 iterations. If the absorption μ were recovered via (27) immediately after steps (1) and (2), the reconstruction would not be satisfactory, as it can be seen in Figure 6e. This makes steps (3a) and (3b) necessary: after repeating step (3) twice, the quality of the reconstruction is sensibly improved (see Figure 6f). The corresponding reconstruction of D is shown in Figure 6d. As anticipated before, the reconstruction of D from u_i is much more stable than that of μ . Note that the absorption was supposed to be known near the boundary of the domain, to avoid problems with the second derivatives in (27).

The case with noise was not studied in this paper, since the robustness to noise of the disjoint sparsity signal separation algorithm has already been tested in § 5.2. The robustness to noise of the other steps of the reconstruction method discussed above is well-known, and standard regularization method can be employed. It is worth noticing that since the absorption μ is found in step (3c) from the reconstructed values of the light intensities u_i , the signal to noise ratio of u_i has to be sufficiently large. Unfortunately, as it can be seen from the third column of Figure 5, the amplitude of the information about μ captured in u_i is very small, and so the noise has to be comparable to this.

6. CONCLUSIONS

In this work we have studied a method for signal separation based on the disjoint sparsity of multiple measurements. A theorem giving unique and stable reconstruction was proved. The result is based on the incoherence of the measurements. Then, the method was applied to hybrid imaging problems, and in particular to quantitative photoacoustic tomography. This technique has been successfully tested on several numerical simulations, and results to be very robust to noise.

The incoherence between the measurements g_i is the main foundation of the method, and the numerical simulations have shown that such property holds true with different solutions to the same PDE, which is the relevant case for hybrid imaging. It would be very interesting to prove this result in general. Randomly chosen boundary conditions may give the necessary incoherence.

Robust Principal Component Analysis (rPCA) [31] might be used as an alternative to the disjoint separation method for the recovery of \tilde{f} and the \tilde{g}_i 's from the knowledge of $h_i = \tilde{f} + \tilde{g}_i$, $i = 1, \dots, N$. Writing $\tilde{f} = A_f \tilde{y}_f$ and $\tilde{g}_i = A_g \tilde{y}_g^i$, the known matrix $M := {}^t A_g [h_1 \ \dots \ h_N]$ can be expressed as

$$M = [{}^t A_g A_f \tilde{y}_f \ \dots \ {}^t A_g A_f \tilde{y}_f] + [\tilde{y}_g^1 \ \dots \ \tilde{y}_g^N],$$

that is the sum of a rank-one matrix and of a sparse matrix. It would be interesting to see whether the requirements for the application of rPCA are fulfilled. Heuristically, this is indeed the case: the incoherence between A_f and A_g should provide the non-sparsity of the low-rank component, while the incoherence, or possibly the disjoint sparsity, of the \tilde{g}_i 's should ensure that the sparse component is not low-rank.

Finally, it would be very interesting to investigate whether the main ideas behind this method can be applied to other inverse problems with multiple measurements consisting of two components, of which only one remains fixed.

APPENDIX A. UNCERTAINTY PRINCIPLES

A.1. Proof of Proposition 2. Let A_f and A_g be as in Proposition 2. For $p = 1, \dots, n$ and $q \in \mathbb{R}^n$ define

$$\xi_p(q) = \max_{1 \leq \alpha_1 < \dots < \alpha_p \leq n} \min_{i=1, \dots, p} |q(\alpha_i)|.$$

Note that $\xi_p(q) > 0$ if and only if $\|q\|_0 \geq p$: in this sense, the map ξ is a quantitative version of the norm $\|\cdot\|_0$. Let $\text{ceil}(z)$ denote the nearest integer greater than or equal to z .

Lemma 2. Take $\zeta = 1, \dots, m_g$ and $p = 1, \dots, n$ such that

$$\|{}^t A_f A_g v\|_0 \geq p, \quad v \in \mathbb{R}^{m_g} \setminus \{0\}, \quad \|v\|_0 \leq \zeta.$$

There exists $C_\xi > 0$ depending only on n, A_f and A_g such that

$$\xi_p({}^t A_f A_g v) \geq C_\xi,$$

for every $v \in \mathbb{R}^{m_g}$ such that $\|v\|_2 = 1$ and $\|v\|_0 \leq \zeta$.

Proof. By contradiction, there exist $v_l \in \mathbb{R}^{m_g}$ such that $\|v_l\|_2 = 1, \|v_l\|_0 \leq \zeta$ and $\xi_p(q_l) \rightarrow 0$ as $l \rightarrow \infty$, where $q_l = {}^t A_f A_g v_l$. Up to a subsequence, we have $v_l \rightarrow v$ for some $v \in \mathbb{R}^{m_g}$ such that $\|v\|_2 = 1$ and $\|v\|_0 \leq \zeta$ and $q_l \rightarrow {}^t A_f A_g v =: q$. By assumption we have $\|q\|_0 \geq p$. Thus, there exist $1 \leq \alpha_1 < \dots < \alpha_p \leq n$ and $\varepsilon > 0$ such that $|q(\alpha_i)| \geq 2\varepsilon$ for every $i = 1, \dots, p$. Since $q_l \rightarrow q$, there exists l_0 such that $|q_l(\alpha_i)| \geq \varepsilon$ for every $i = 1, \dots, p$ and every $l \geq l_0$. Hence $\xi_p(q_l) \geq \varepsilon$ for every $l \geq l_0$, a contradiction. \square

We are now in a position to prove Proposition 2.

Proof of Proposition 2. Define $D = (\sqrt{m_g} + \frac{2}{3})(1 + C_\xi^{-1})$ and take $q \in \mathbb{R}^n$ such that $\|A_f q\|_2 > D$ and $\|{}^t A_g^\perp A_f q\|_2 \leq \frac{2}{3}$. Write ${}^t A_g A_f q = v + r$ where

$$v(\alpha) = \begin{cases} {}^t A_g A_f q(\alpha) & \text{if } |{}^t A_g A_f q(\alpha)| \geq 1, \\ 0 & \text{otherwise.} \end{cases}$$

Thus $\|r\|_\infty \leq 1$, whence $\|r\|_2 \leq \sqrt{m_g}$. Therefore, by the estimate

$$D < \|A_f q\|_2 = (\|{}^t A_g A_f q\|_2^2 + \|{}^t A_g^\perp A_f q\|_2^2)^{\frac{1}{2}} \leq \|{}^t A_g A_f q\|_2 + \frac{2}{3},$$

and by construction of D we obtain

$$(28) \quad \|v\|_2 \geq \|{}^t A_g A_f q\|_2 - \|r\|_2 > D - (\sqrt{m_g} + \frac{2}{3}) = (\sqrt{m_g} + \frac{2}{3})C_\xi^{-1} > 0.$$

Set $v' := v/\|v\|_2$, $\zeta := \|v'\|_0$ and $p = \text{ceil}(2/M) - \zeta$. By Lemma 2, whose assumptions are satisfied by Proposition 1 (using that $A_f {}^t A_f = I$), we have $\xi_p({}^t A_f A_g v') \geq C_\xi$. Thus, there exist $1 \leq \alpha_1 < \dots < \alpha_p \leq n$ such that

$$(29) \quad |{}^t A_f A_g v'(\alpha_i)| \geq C_\xi, \quad \text{for every } i = 1, \dots, p.$$

From the identity $A_f q = A_g({}^t A_g A_f q) + A_g^\perp({}^t A_g^\perp A_f q)$, setting $z = {}^t A_f(A_g r + A_g^\perp({}^t A_g^\perp A_f q))$ we obtain

$$q = ({}^t A_f A_g v')\|v\|_2 + z.$$

In view of Lemma 1 parts 1 and 2 we have

$$\|z\|_\infty \leq \|z\|_2 \leq \|A_g r + A_g^\perp({}^t A_g^\perp A_f q)\|_2 \leq \|r\|_2 + \|{}^t A_g^\perp A_f q\|_2 \leq \sqrt{m_g} + \frac{2}{3}.$$

As a result, by (29) and (28) and the expression for D we have

$$|q(\alpha_i)| = \|v\|_2 ({}^t A_f A_g v')(\alpha_i) + z(\alpha_i) \geq \|v\|_2 C_\xi - (\sqrt{m_g} + \frac{2}{3}) > 0$$

for every $i = 1, \dots, p$. Therefore

$$\|q\|_0 + \|v\|_0 \geq p + \zeta \geq 2/M.$$

Finally, the conclusion follows from the equality $\#\{\alpha : |({}^t A_g A_f q)(\alpha)| \geq 1\} = \|v\|_0$. \square

A.2. Proof of Proposition 3. Let us first discuss the orthobasis of 2D Haar wavelets of $\mathbb{R}^{d \times d}$, where $d = 2^J$. A_f is constructed via translations and dilations of four types of wavelets, as we now describe. Let $j = 1, \dots, J-1$ denote the scale, from the finest to the coarsest and let $k_1, k_2 = 1, \dots, 2^{J-j}$ be the horizontal and vertical translation parameters. We consider four families of atoms $\psi_{j,k}^i$ defined by

$$\begin{cases} \psi_{j,k}^1(2^j(k_1-1) + \alpha_1, 2^j(k_2-1) + \alpha_2) = -2^{-j}, & \alpha_1 = 1, \dots, 2^j, \\ \psi_{j,k}^1(2^j(k_1-1) + \alpha_1, 2^j(k_2-1) + 2^{j-1} + \alpha_2) = 2^{-j}, & \alpha_2 = 1, \dots, 2^{j-1}, \\ \psi_{j,k}^2(2^j(k_1-1) + \alpha_1, 2^j(k_2-1) + \alpha_2) = -2^{-j}, & \alpha_1 = 1, \dots, 2^{j-1}, \\ \psi_{j,k}^2(2^j(k_1-1) + 2^{j-1} + \alpha_1, 2^j(k_2-1) + \alpha_2) = 2^{-j}, & \alpha_2 = 1, \dots, 2^j, \\ \psi_{j,k}^3(2^j(k_1-1) + 2^{j-1} + \alpha_1, 2^j(k_2-1) + \alpha_2) = -2^{-j}, & \\ \psi_{j,k}^3(2^j(k_1-1) + \alpha_1, 2^j(k_2-1) + 2^{j-1} + \alpha_2) = -2^{-j}, & \alpha_1 = 1, \dots, 2^{j-1}, \\ \psi_{j,k}^3(2^j(k_1-1) + \alpha_1, 2^j(k_2-1) + \alpha_2) = 2^{-j}, & \alpha_2 = 1, \dots, 2^{j-1}, \\ \psi_{j,k}^3(2^j(k_1-1) + 2^{j-1} + \alpha_1, 2^j(k_2-1) + 2^{j-1} + \alpha_2) = 2^{-j}, & \\ \psi_{j,k}^4(2^j(k_1-1) + \alpha_1, 2^j(k_2-1) + \alpha_2) = 2^{-j}, & \alpha_1, \alpha_2 = 1, \dots, 2^j, \end{cases}$$

and zero elsewhere. The orthonormal basis of Haar wavelets A_f is given by

$$\bigcup_{j=1}^{J-2} \{\psi_{j,k}^i : i = 1, 2, 3, k \in \{1, \dots, 2^{J-j}\}^2\} \cup \{\psi_{J-1,k}^i : i = 1, \dots, 4, k \in \{1, 2\}^2\}.$$

The proof of Proposition 3 is based on the following result.

Lemma 3. *Under the assumptions of Proposition 3, for every $v \in \mathbb{R}^{m_g} \setminus \{0\}$ we have*

$$\|{}^t A_f A_g v\|_0 \geq \sum_{j=1}^{J-B-1} (2^{J-j} - 2L)^2$$

Proof. Write $g = A_g v$. By construction of A_g , the vector g can be written as a linear combination of low frequency real sinusoids, namely

$$g = \sum_{i=1}^4 \sum_{l_1, l_2=0}^L \gamma_l^i \chi_l^i$$

for some weights $\gamma_l^i \in \mathbb{R}$. Using standard trigonometric equalities, we can write the above sum in terms of complex sinusoids

$$g(\alpha) = \sum_{l_1, l_2=-L}^L \theta_l e^{2\pi i l_1 \frac{\alpha_1}{2^j}} e^{2\pi i l_2 \frac{\alpha_2}{2^j}}, \quad \alpha \in \{1, \dots, 2^J\}^2.$$

for some complex weights $\theta_l \in \mathbb{C}$. Since the constant vector is not in A_g and $v \neq 0$, we have that $\theta_l \neq 0$ for some $l \neq (0, 0)$. Without loss of generality, we can assume that there exists $l^* \in \{-L, \dots, L\}^2$ such that

$$(30) \quad \theta_{l^*} \neq 0, \quad l_2^* \neq 0.$$

By construction of A_f we have that

$$(31) \quad \|{}^t A_f g\|_0 \geq \sum_{j=1}^{J-B-1} \#\{k \in \{1, \dots, 2^{J-j}\}^2 : (g, \psi_{j,k}^1)_2 \neq 0\} =: \sum_{j=1}^{J-B-1} \#T_j$$

We now want to find a lower bound for $\#T_j$.

Fix $j = 1, \dots, J - B - 1$. For simplicity of notation, set $e_{l_i}(\cdot) = e^{2\pi i l_i \frac{\cdot}{2^j}}$ and $m_{k_i} = 2^j(k_i - 1)$. For $k \in \{1, \dots, 2^{J-j}\}^2$ we have

$$\begin{aligned} 2^j(g, \psi_{j,k}^1)_2 &= \sum_{l_1, l_2 = -L}^L \sum_{\alpha_1=1}^{2^j} \sum_{\alpha_2=1}^{2^{j-1}} \theta_l(e_{l_1}(m_{k_1} + \alpha_1)e_{l_2}(m_{k_2} + 2^{j-1} + \alpha_2) \\ &\quad - e_{l_1}(m_{k_1} + \alpha_1)e_{l_2}(m_{k_2} + \alpha_2)) \\ &= \sum_{l_1, l_2 = -L}^L \theta_l e_{l_1}(m_{k_1})e_{l_2}(m_{k_2}) \sum_{\alpha_1=1}^{2^j} \sum_{\alpha_2=1}^{2^{j-1}} e_{l_1}(\alpha_1)e_{l_2}(\alpha_2)(e_{l_2}(2^{j-1}) - 1) \\ &= \sum_{l_2 = -L}^L \zeta_{l_2}(k_1)e_{l_2}(m_{k_2}) \end{aligned}$$

where we have set

$$\zeta_{l_2}(k_1) = \sum_{l_1 = -L}^L \theta_l(e_{l_2}(2^{j-1}) - 1) \left(\sum_{\alpha_2=1}^{2^{j-1}} e_{l_2}(\alpha_2) \right) \left(\sum_{\alpha_1=1}^{2^j} e_{l_1}(\alpha_1) \right) e_{l_1}(m_{k_1}).$$

Since $L < 2^B$ with $B \leq J - 2$ and $j \leq J - B - 1$, by using standard identities for geometric sums it is easy to show that $(e_{l_2}(2^{j-1}) - 1) \left(\sum_{\alpha_2=1}^{2^{j-1}} e_{l_2}(\alpha_2) \right) \left(\sum_{\alpha_1=1}^{2^j} e_{l_1}(\alpha_1) \right) \neq 0$ for all l_1 and all $l_2 \neq 0$. As a result, in view of (30) we have that the polynomial in the complex variable z

$$p_{l_2^*} = \sum_{l_1 = -L}^L \theta_{l_1, l_2^*} (e_{l_2^*}(2^{j-1}) - 1) \left(\sum_{\alpha_2=1}^{2^{j-1}} e_{l_2^*}(\alpha_2) \right) \left(\sum_{\alpha_1=1}^{2^j} e_{l_1}(\alpha_1) \right) z^{l_1+L}$$

is non trivial. By the fundamental theorem of algebra, it has at most $2L$ zeros. Therefore, writing $z = e^{2\pi i m_{k_1} 2^{-j}}$, we obtain that $\#E_j \geq 2^{J-j} - 2L$, where $E_j = \{k_1 \in \{1, \dots, 2^{J-j}\} : \zeta_{l_2^*}(k_1) \neq 0\}$. Take now $k_1 \in E_j$. Arguing in a similar way and writing $z = e^{2\pi i m_{k_2} 2^{-j}}$, we have that

$$e_L(m_{k_2}) 2^j(g, \psi_{j,k}^1)_2 = \sum_{l_2 = -L}^L \zeta_{l_2}(k_1) z^{l_2+L}.$$

Since $\zeta_{l_2^*}(k_1) \neq 0$, this polynomial in z is non trivial, and so has at most $2L$ zeros. In other words, for $k_1 \in E_j$ we have that

$$\#\{k_2 \in \{1, \dots, 2^{J-j}\} : (g, \psi_{j,k}^1)_2 \neq 0\} \geq 2^{J-j} - 2L.$$

Recalling that $\#E_j \geq 2^{J-j} - 2L$, this implies that $\#T_j \geq (2^{J-j} - 2L)^2$. Finally, the result immediately follows from (31). \square

We are now ready to prove Proposition 3. The proof follows the same argument used for Proposition 2.

Proof of Proposition 3. Define $D = \frac{2}{3}(1 + C_\xi^{-1})$ (where C_ξ is given by Lemma 2) and take $q \in \mathbb{R}^n$ with $\|A_f q\|_2 > D$ and $\|{}^t A_g^\perp A_f q\|_2 \leq 2/3$. Lemma 1 part 1 and the identity $A_f q = A_g({}^t A_g A_f q) + A_g^\perp({}^t A_g^\perp A_f q)$ yield

$$D < \|A_f q\|_2 = \left(\|{}^t A_g A_f q\|_2^2 + \|{}^t A_g^\perp A_f q\|_2^2 \right)^{\frac{1}{2}} \leq \|{}^t A_g A_f q\|_2 + 2/3$$

whence by construction of D we obtain

$$(32) \quad \| {}^t A_g A_f q \|_2 > 2C_\xi^{-1}/3.$$

Set $v = {}^t A_g A_f q / \| {}^t A_g A_f q \|_2$. By Lemma 3, the assumptions of Lemma 2 are satisfied with $p = \sum_{j=1}^{J-B-1} (2^{J-j} - 2L)^2$ and $\zeta = m_g$; as a result $\xi_p({}^t A_f A_g v) \geq C_\xi$. In other words, there exist $\alpha_1 < \dots < \alpha_p$ such that $|({}^t A_f A_g v)(\alpha_i)| \geq C_\xi$. Moreover, by Lemma 1 parts 1 and 2 we have $\| {}^t A_f A_g^\perp {}^t A_g^\perp A_f q \|_2 \leq 2/3$, whence $\| {}^t A_f A_g^\perp {}^t A_g^\perp A_f q \|_\infty \leq 2/3$. As a consequence, by (32) and the identity $q = \| {}^t A_g A_f q \|_2 {}^t A_f A_g v + {}^t A_f A_g^\perp {}^t A_g^\perp A_f q$ we obtain

$$|q(\alpha_i)| \geq \| {}^t A_g A_f q \|_2 |{}^t A_f A_g v(\alpha_i)| - |{}^t A_f A_g^\perp {}^t A_g^\perp A_f q(\alpha_i)| > \frac{2}{3} C_\xi^{-1} C_\xi - \frac{2}{3} = 0,$$

for every $i = 1, \dots, p$. In other words, $\|q\|_0 \geq p$, as desired. \square

REFERENCES

- [1] G. S. Alberti. On multiple frequency power density measurements. *Inverse Problems*, 29(11):115007, 25, 2013.
- [2] G. S. Alberti. Enforcing local non-zero constraints in pdes and applications to hybrid imaging problems. *Communications in Partial Differential Equations*, 40(10):1855–1883, 2015.
- [3] G. S. Alberti. On multiple frequency power density measurements II. The full Maxwell's equations. *Journal of Differential Equations*, 258(8):2767 – 2793, 2015.
- [4] G. S. Alberti, H. Ammari, and K. Ruan. Multi-frequency acousto-electromagnetic tomography. *Contemp. Math. (to appear)*.
- [5] G. S. Alberti and Y. Capdeboscq. A propos de certains problèmes inverses hybrides. In *Seminaire: Equations aux Dérivées Partielles. 2013–2014*, Sémin. Équ. Dériv. Partielles, page Exp. No. II. École Polytech., Palaiseau.
- [6] G. S. Alberti and Y. Capdeboscq. *Lectures on elliptic methods for hybrid inverse problems*. In preparation.
- [7] H. Ammari. *An Introduction to Mathematics of Emerging Biomedical Imaging*, volume 62 of *Math. Appl.* Springer-Verlag, Berlin, 2008.
- [8] H. Ammari, E. Bonnetier, Y. Capdeboscq, M. Tanter, and M. Fink. Electrical impedance tomography by elastic deformation. *SIAM J. Appl. Math.*, 68(6):1557–1573, 2008.
- [9] H. Ammari, E. Bossy, J. Garnier, L. H. Nguyen, and L. Seppecher. Reconstruction of a piecewise smooth absorption coefficient by an acousto-optic process. *Comm. Part. Diff. Equat.*, 38(10):1737–1762, 2013.
- [10] H. Ammari, E. Bossy, J. Garnier, L. H. Nguyen, and L. Seppecher. A reconstruction algorithm for ultrasound-modulated diffuse optical tomography. *Proc. Amer. Math. Soc.*, 142(9):3221–3236, 2014.
- [11] H. Ammari, E. Bossy, V. Jugnon, and H. Kang. Mathematical modeling in photoacoustic imaging of small absorbers. *SIAM Rev.*, 52(4):677–695, 2010.
- [12] H. Ammari, E. Bossy, V. Jugnon, and H. Kang. Reconstruction of the optical absorption coefficient of a small absorber from the absorbed energy density. *SIAM J. Appl. Math.*, 71(3):676–693, 2011.
- [13] H. Ammari, Y. Capdeboscq, F. de Gournay, A. Rozanova-Pierrat, and F. Triki. Microwave imaging by elastic deformation. *SIAM J. Appl. Math.*, 71(6):2112–2130, 2011.
- [14] H. Ammari, J. Garnier, W. Jing, and L. H. Nguyen. Quantitative thermo-acoustic imaging: An exact reconstruction formula. *J. Differential Equations*, 254(3):1375–1395, 2013.
- [15] H. Ammari, L. H. Nguyen, and L. Seppecher. Reconstruction and stability in acousto-optic imaging for absorption maps with bounded variation. *J. Funct. Anal.*, 267(11):4361–4398, 2014.
- [16] G. Bal. Hybrid inverse problems and internal functionals. In G. Uhlmann, editor, *Inverse problems and applications: inside out. II*, volume 60 of *Math. Sci. Res. Inst. Publ.*, pages 325–368. Cambridge Univ. Press, Cambridge, 2013.
- [17] G. Bal, E. Bonnetier, F. Monard, and F. Triki. Inverse diffusion from knowledge of power densities. *Inverse Probl. Imaging*, 7(2):353–375, 2013.

- [18] G. Bal, A. Jollivet, and V. Jugnon. Inverse transport theory of photoacoustics. *Inverse Problems*, 26(2):025011, 35, 2010.
- [19] G. Bal and K. Ren. Multi-source quantitative photoacoustic tomography in a diffusive regime. *Inverse Problems*, 27(7):075003, 20, 2011.
- [20] G. Bal and K. Ren. On multi-spectral quantitative photoacoustic tomography in diffusive regime. *Inverse Problems*, 28(2):025010, 13, 2012.
- [21] G. Bal and G. Uhlmann. Inverse diffusion theory of photoacoustics. *Inverse Problems*, 26(8):085010, 20, 2010.
- [22] T. Blumensath and M. E. Davies. Iterative thresholding for sparse approximations. *J. Fourier Anal. Appl.*, 14(5-6):629–654, 2008.
- [23] J. Bobin, Y. Moudden, J. Fadili, and J.-L. Starck. Morphological diversity and sparsity for multichannel data restoration. *J. Math. Imaging Vision*, 33(2):149–168, 2009.
- [24] J. Bobin, Y. Moudden, and J.-L. Starck. Enhanced source separation by morphological component analysis. In *Acoustics, Speech and Signal Processing, 2006. ICASSP 2006 Proceedings. 2006 IEEE International Conference on*, volume 5, pages V–V, May 2006.
- [25] P. Bofill and M. Zibulevsky. Underdetermined blind source separation using sparse representations. *Signal Processing*, 81(11):2353 – 2362, 2001.
- [26] A. G. Bruce, S. Sardy, and P. Tseng. Block coordinate relaxation methods for nonparametric signal denoising. *Proc. SPIE*, 3391:75–86, 1998.
- [27] A. M. Bruckstein, D. L. Donoho, and M. Elad. From sparse solutions of systems of equations to sparse modeling of signals and images. *SIAM Rev.*, 51(1):34–81, 2009.
- [28] L. Calatroni, C. Chung, J. C. De Los Reyes, C.-B. Schönlieb, and T. Valkonen. Bilevel approaches for learning of variational imaging models. *ArXiv e-prints*, May 2015.
- [29] E. J. Candès and D. L. Donoho. Ridgelets: a key to higher-dimensional intermittency? *Philosophical Transactions of the Royal Society of London A: Mathematical, Physical and Engineering Sciences*, 357(1760):2495–2509, 1999.
- [30] E. J. Candès and D. L. Donoho. New tight frames of curvelets and optimal representations of objects with piecewise C^2 singularities. *Comm. Pure Appl. Math.*, 57(2):219–266, 2004.
- [31] E. J. Candès, X. Li, Y. Ma, and J. Wright. Robust principal component analysis? *J. ACM*, 58(3):11:1–11:37, June 2011.
- [32] E. J. Candès and J. Romberg. Quantitative robust uncertainty principles and optimally sparse decompositions. *Foundations of Computational Mathematics*, 6(2):227–254, 2006.
- [33] Y. Capdeboscq, J. Fehrenbach, F. de Gournay, and O. Kavian. Imaging by modification: numerical reconstruction of local conductivities from corresponding power density measurements. *SIAM J. Imaging Sci.*, 2(4):1003–1030, 2009.
- [34] A. Chambolle. An algorithm for total variation minimization and applications. *Journal of Mathematical Imaging and Vision*, 20(1-2):89–97, 2004.
- [35] J. Chen and X. Huo. Theoretical results on sparse representations of multiple-measurement vectors. *Signal Processing, IEEE Transactions on*, 54(12):4634–4643, Dec 2006.
- [36] S. S. Chen, D. L. Donoho, and M. A. Saunders. Atomic decomposition by basis pursuit. *SIAM Rev.*, 43(1):129–159, 2001. Reprinted from *SIAM J. Sci. Comput.* **20** (1998), no. 1, 33–61 (electronic) [MR1639094 (99h:94013)].
- [37] S. Cotter, B. Rao, K. Engan, and K. Kreutz-Delgado. Sparse solutions to linear inverse problems with multiple measurement vectors. *Signal Processing, IEEE Transactions on*, 53(7):2477–2488, July 2005.
- [38] B. Cox, T. Tarvainen, and S. Arridge. Multiple illumination quantitative photoacoustic tomography using transport and diffusion models. In *Tomography and inverse transport theory*, volume 559 of *Contemp. Math.*, pages 1–12. Amer. Math. Soc., Providence, RI, 2011.
- [39] B. T. Cox, S. R. Arridge, K. P. Köstli, and P. C. Beard. Two-dimensional quantitative photoacoustic image reconstruction of absorption distributions in scattering media by use of a simple iterative method. *Appl. Opt.*, 45(8):1866–1875, Mar 2006.
- [40] B. T. Cox, J. G. Laufer, and P. C. Beard. The challenges for quantitative photoacoustic imaging, 2009.
- [41] T. Ding, K. Ren, and S. Vallélian. A one-step reconstruction algorithm for quantitative photoacoustic imaging. *Preprint*, 2015.
- [42] D. Donoho and G. Kutyniok. Microlocal analysis of the geometric separation problem. *Comm. Pure Appl. Math.*, 66(1):1–47, 2013.

- [43] D. Donoho, Y. Tsaig, I. Drori, and J.-L. Starck. Sparse solution of underdetermined systems of linear equations by stagewise orthogonal matching pursuit. *Information Theory, IEEE Transactions on*, 58(2):1094–1121, Feb 2012.
- [44] D. L. Donoho and M. Elad. Optimally sparse representation in general (nonorthogonal) dictionaries via l^1 minimization. *Proc. Natl. Acad. Sci. USA*, 100(5):2197–2202 (electronic), 2003.
- [45] D. L. Donoho and X. Huo. Uncertainty principles and ideal atomic decomposition. *IEEE Trans. Inform. Theory*, 47(7):2845–2862, 2001.
- [46] D. L. Donoho and P. B. Stark. Uncertainty principles and signal recovery. *SIAM Journal on Applied Mathematics*, 49(3):906–931, 1989.
- [47] M. Elad and A. M. Bruckstein. A generalized uncertainty principle and sparse representation in pairs of bases. *IEEE Trans. Inform. Theory*, 48(9):2558–2567, 2002.
- [48] M. Elad, J.-L. Starck, P. Querre, and D. L. Donoho. Simultaneous cartoon and texture image inpainting using morphological component analysis (MCA). *Appl. Comput. Harmon. Anal.*, 19(3):340–358, 2005.
- [49] H. Gao, S. Osher, and H. Zhao. Quantitative photoacoustic tomography. In *Mathematical modeling in biomedical imaging. II*, volume 2035 of *Lecture Notes in Math.*, pages 131–158. Springer, Heidelberg, 2012.
- [50] P. Georgiev, F. Theis, and A. Cichocki. Sparse component analysis and blind source separation of underdetermined mixtures. *Neural Networks, IEEE Transactions on*, 16(4):992–996, July 2005.
- [51] M. Haltmeier, L. Neumann, and S. Rabanser. Single-stage reconstruction algorithm for quantitative photoacoustic tomography. *Inverse Problems*, 31(6):065005, 2015.
- [52] P. Kittipoom, G. Kutyniok, and W.-Q. Lim. Construction of compactly supported shearlet frames. *Constr. Approx.*, 35(1):21–72, 2012.
- [53] P. Kuchment. Mathematics of hybrid imaging: A brief review. In I. Sabadini and D. C. Struppa, editors, *The Mathematical Legacy of Leon Ehrenpreis*, volume 16 of *Springer Proceedings in Mathematics*, pages 183–208. Springer Milan, 2012.
- [54] P. Kuchment and L. Kunyansky. Mathematics of photoacoustic and thermoacoustic tomography. In O. Scherzer, editor, *Handbook of Mathematical Methods in Imaging*, pages 817–865. Springer New York, 2011.
- [55] G. Kutyniok. Data separation by sparse representations. In *Compressed sensing*, pages 485–514. Cambridge Univ. Press, Cambridge, 2012.
- [56] G. Kutyniok. Geometric separation by single-pass alternating thresholding. *Appl. Comput. Harmon. Anal.*, 36(1):23–50, 2014.
- [57] G. Kutyniok and W.-Q. Lim. Compactly supported shearlets are optimally sparse. *J. Approx. Theory*, 163(11):1564–1589, 2011.
- [58] D. Labate, W.-Q. Lim, G. Kutyniok, and G. Weiss. Sparse multidimensional representation using shearlets. *Proc. SPIE*, 5914:59140U–59140U–9, 2005.
- [59] S. Mallat and Z. Zhang. Matching pursuits with time-frequency dictionaries. *Signal Processing, IEEE Transactions on*, 41(12):3397–3415, Dec 1993.
- [60] M. B. McCoy and J. A. Tropp. The achievable performance of convex demixing. *ArXiv e-prints*, Sept. 2013.
- [61] W. Naetar and O. Scherzer. Quantitative photoacoustic tomography with piecewise constant material parameters. *SIAM J. Imaging Sci.*, 7(3):1755–1774, 2014.
- [62] A. Pulkkinen, B. T. Cox, S. R. Arridge, J. P. Kaipio, and T. Tarvainen. A Bayesian approach to spectral quantitative photoacoustic tomography. *Inverse Problems*, 30(6):065012, 18, 2014.
- [63] K. Ren, H. Gao, and H. Zhao. A hybrid reconstruction method for quantitative PAT. *SIAM J. Imaging Sci.*, 6(1):32–55, 2013.
- [64] A. Rosenthal, D. Razansky, and V. Ntziachristos. Quantitative optoacoustic signal extraction using sparse signal representation. *Medical Imaging, IEEE Transactions on*, 28(12):1997–2006, Dec 2009.
- [65] R. Rubinstein, A. Bruckstein, and M. Elad. Dictionaries for sparse representation modeling. *Proceedings of the IEEE*, 98(6):1045–1057, June 2010.
- [66] L. I. Rudin, S. Osher, and E. Fatemi. Nonlinear total variation based noise removal algorithms. *Physica D: Nonlinear Phenomena*, 60(1-4):259 – 268, 1992.
- [67] J. K. Seo and E. J. Woo. *Nonlinear Inverse Problems in Imaging*. Wiley, 2013.

- [68] P. Shao, B. Cox, and R. J. Zemp. Estimating optical absorption, scattering, and grüneisen distributions with multiple-illumination photoacoustic tomography. *Appl. Opt.*, 50(19):3145–3154, Jul 2011.
- [69] J.-L. Starck, M. Elad, and D. Donoho. Redundant multiscale transforms and their application for morphological component separation. In *Advances in Imaging and Electron Physics*, volume 132 of *Advances in Imaging and Electron Physics*, pages 287 – 348. Elsevier, 2004.
- [70] J.-L. Starck, M. Elad, and D. Donoho. Image decomposition via the combination of sparse representations and a variational approach. *Image Processing, IEEE Transactions on*, 14(10):1570–1582, Oct 2005.
- [71] I. Touni, S. Caldarelli, and B. Torrèsani. A review of blind source separation in NMR spectroscopy. *Progress in Nuclear Magnetic Resonance Spectroscopy*, 81(0):37 – 64, 2014.
- [72] J. Tropp. Greed is good: algorithmic results for sparse approximation. *Information Theory, IEEE Transactions on*, 50(10):2231–2242, Oct 2004.

DEPARTMENT OF MATHEMATICS AND APPLICATIONS, ÉCOLE NORMALE SUPÉRIEURE, 45 RUE D'ULM, 75005 PARIS, FRANCE.

E-mail address: `giovanni.alberti@ens.fr`

DEPARTMENT OF MATHEMATICS AND ET APPLICATIONS, ÉCOLE NORMALE SUPÉRIEURE, 45 RUE D'ULM, 75005 PARIS, FRANCE.

E-mail address: `habib.ammari@ens.fr`